Diploma Thesis

Development of a Battery Test System

Stefan Gruber

Institute of Electrical Measurement and Measurement Signal Processing

Graz University of Technology

Head of the Institute: Univ.-Prof. Dipl.-Ing.Dr.techn. Georg Brasseur

Advisor: Dipl.-Ing.Dr.techn. Hannes Wegleiter

October 2012

Abstract

For the development of meaningful battery models, an extensive testing of battery cells is essential. Depending on the application and the desired accuarcy, the model should considerate temperature influence, aging as well as cycle age among others. Therefore, it is necessary to ensure an accurant measurement and to offer a high charge and discharge rate. The current available comercial systems are either only cyclers or measuring instruments for impedance spectroscopy. Moreover, both systems do possess a relatively large requirement of space.

The current thesis is concerned with the development of a small battery test system which is applicable for a wide range. Hence, it should be able to charge and discharge the cell at an reasonable rate ($\pm$ 50 A). Furthermore, the measurement of the battery voltage and current must have a wide frequencey range (50 µHz - 10 kHz) to develop a battery model.

The theoretical part is dealing with required battery basics regarding different battery types, the temperature influence and the charge and discharge characteristics. Further, a short overview of modeling with impedance spectroscopy is given.

The practical part describes the development and implementation of the desired battery test system consisting of an amplifier unit and a measurement and control unit. On the basis of experiments the strengths and weaknesses of the system are shown.

Finally, the results of the measurement are discussed and suggestions to improve the performance of the measurement system are given.

Zusammenfassung

Für die Entwicklung aussagekräftiger Batteriemodelle ist eine umfangreiche Testung von Batteriezellen unerlässlich. Je nach Anwendung und gewünschter Genauigkeit, muss das Modell unter anderem die Temperatureinflüsse, die zeitliche sowie die ladezyklische Alterung berücksichtigen. Dafür ist es notwendig die Batterien sowohl vermessen als auch belasten zu können. Die derzeitig am Markt erhältlichen kommerziellen Systeme sind entweder Zyklisierer oder Messgeräte zur Impedanzspektroskopie und benötigen einen großen Platzbedarf.

Ziel dieser Arbeit ist es, ein möglichst universelles und platzsparendes Batterietestsystem zu entwickeln, das in der Lage ist, die Batteriezelle mit ausreichend starken Strömen zu laden und entladen (± 50 A). Zudem ist es essentiell, Strom und Spannung in einem breiten Frequenzbereich (50 µHz - 10 kHz) zu messen, um mithilfe der Impedanzspektroskopie Batteriemodelle entwickeln zu können.

Der theoretische Teil der Arbeit befasst sich mit den notwendigen Grundlagen hinsichtlich der verschiedenen Batterietypen, den Temperatureinfluss, sowie deren Lade- und Entladeverhalten. Weiters wird ein kurzer Überblick über die Modellbildung mittels Impedanzspektroskopie gegeben.

Der praktische Teil der Arbeit beschäftigt sich mit der Entwicklung und Umsetzung eines Prototypen, der aus einer Verstärkereinheit und einer Kontroll- und Messeinheit besteht. Anhand von Experimenten mit den einzelnen Einheiten, sowie dem Gesamtsystem, werden dessen Stärken und Schwächen ermittelt.

Den Abschluss der Arbeit bildet die Diskussion der Messergebnisse und Vorschläge zur Verbesserung der Leistungsfähigkeit des Messsystems.

Statutory declaration

I declare that I have authored this thesis independently, that I have not used other than the declared sources / resources, and that I have explicitly marked all material which has been quoted either literally or by content from the used sources.

Place	Date	Signature

Contents

1 Introduction

Batteries are used as power source for portable devices like torches, radios, watches, electronic keys and remote controls for ages. Further, the need of advanced rechargeable batteries for e.g. smart phones, laptops, music players is constantly increasing. Every application has its own battery demands in terms of capacity, volume, weight, costs and reachargeability. Hence, the capacity differs from a few Wh for consumer portable devices to several kWh for hybrid electrical vehicles (HEV) and electrical vehicles (EV).

A study from Frost & Sullivan in 2009[1] investigated the battery market and figured out that already 37% of the revenue contributions in 2009 are done by lithium-ion batteries. Figure 1.1 shows the global battery market in terms of revenue contributions by different battery chemistries. In comparison to the well-known lead-acid batteries (in vehicles and stationary applications), the lithium-ion batteries have reached a comparable size on the market. Considering the advancing electrification of vehicles the study predicts that the market for lithium-ion batteries will grow further.

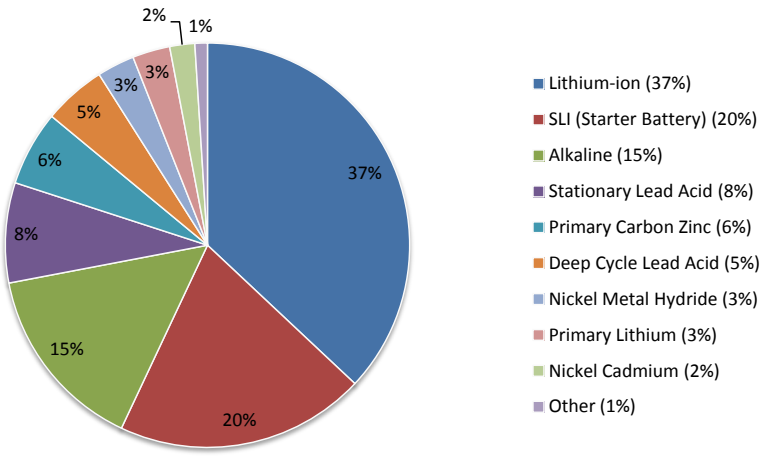

Figure 1.1: Global battery market (revenue contribution) by different battery chemistries in 2009 .

The upcoming of hybrid electric and electric cars is also directed by the policies of countries against climate change and air pollution. One example can be seen in the AB 32, the Global Warming Solutions Act of 2006 [2], in California. One part focuses on the reduction of greenhouse gases produced by cars and the support of zero

emission vehicles [3]. Another example is the European Roadmap for Electrification of Road Transport from November 2010 [4].

However, the new coming developments including electric and electric hybrid vehicles and the storage of electric energy produced by renewable energies such as wind and solar generators require batteries with special characteristics. Since the portable electronic became a mass product, not only the performance of the battery, but also the expense factor is essential. Philip C. Symons and Paul C. Butler define the needs of EVs, HEVs, electric-utility applications and portable devices as follows[5, page 1188]:

Electric vehicle batteries need:
(1) high specific energy and energy density to provide adequate vehicle driving range
(2) high power density to provide acceleration
(3) long cycle life with little maintenance
(4) low cost.

On the other hand, batteries for hybrid electric vehicles require:
(1) very high specific power and power density to provide acceleration
(2) capability of accepting high power repetitive charges from regenerative braking
(3) very long cycle life with no maintenance under shallow cycling conditions
(4) moderate cost.

Batteries for electric-utility applications must have:
(1) low first cost
(2) high reliability when operated in megawatt-hour-size systems at 2000 V or more
(3) high volumetric energy and power densities.

Portable electronic devices require low-cost and readily available, lightweight batteries that have both high specific energy and power and high energy and power densities. Safe operation and minimal environmental impact during manufacturing, use and disposal are mandatory for all applications.

In order to build HEVs and EVs new control algorithms must be developed. Furthermore, some simulation environment is necessary to optimize the required components. Therefore, accurate models of all vehicle components are mandatory, especially the battery itself. Due to the lack of experience with long-term suitability of lithium-ion batteries for automotive use in electric powertrains, no empirical data exist. A comprehensive evalution of the batteries in terms of performance, cycle life and long-term operating cost is desirable. Hence, accurate information about the customers' driving behaviour and the climate conditions they live in should be acquired. Meanwhile, we have to rely on testing equipments, calculations, estimations and simulations.

The currently available comercial systems are either only cyclers or instruments for impedance spectroscopy measuring. Moreover, both Systems have a relatively large weight and space requirement. The next section will include a brief overview of available systems and their features:

- Gamry Instruments - Reference 3000^{TM}[6]
  The Reference 3000^{TM}is an AC impedance measurement instrument. It consists of a high-performance Potentiostat/Galvanostat/ZRA with a maximum current of ± 3 A, a maximum voltage of ± 32 V, a frequency measurement range of 10 µHz to 1 MHz and a measurement accuracy of ± 1 mV ± 0.3 % of reading and ± 10 pA ± 0.3 % of range.
- PEC - SBT0550[7]
  The SBT0550 is a 24-channel battery tester. Every channel is independent, controlled by a microprocessor and uses a MOSFET to obtain a high accuracy, reliability and flexibility. 24 channels of 5 V, 50 A are mounted in 1 test rack. The voltage and current is measured with a resolution of 100 µV and 1 µA to 1 mA at a sampling frequency of 1 kHz.
- Arbin Instruments - BT-2000[8]
  The BT2000 is a custom-designed multi-channel battery testing system. It can be applied to battery testing, material research, electrode study, fuel cell testing, supercapacitor R&D, or electrochemical investigation. Depending on the system configuration various charge/discharge currents from ± 10 nA up to several ± kA from below 0 V to 800 V are possible. The measurement resolution is normally 16 bit.
- Maccor - FRA-0355[9]
  The FRA-0355 Frequency Response Analyzer is a AC impedance measurement instrument. It consists of a Potentiostat/Galvanostat/ZRA with a maximum current of ± 3 A, a maximum voltage of ± 55 V and a frequency measurement rage of 1 mHz to 30 kHz. Furthermore, the FRA can accurately output and measure an AC signal as low as 100 µV peak-to-peak.
- Maccor - Series 8500[10]
  The Series 8500 is a test system designed for testing the performance characteristics of EV, HEV, PHEV and energy storage batteries. Possible configurations allow charge/discharge currents from 100 to 1000 A and a voltage from 50 to 500 V. Moreover, the system has a 16 bit resolution and the data is collected every 20 ms.

1.1 Problem description and requirements

The purpose of this thesis is the development and realisation of a prototype to test a single battery cell focussing lithium-ion batteries. The prototype should work with a wide range of existing and new developing batteries with a cell voltage up to 5 V. The investigated battery cell should be stressed with high (from 0 to 50 A) charge and discharge currents to study the behaviour of the battery in terms of health and aging. Therefore, the prototype should be able to test a battery cell over weeks, i.e., safety and self-shut-down features must be implemented. To allow

research in battery modeling regarding impedance spectroscopy, the prototype must be able to measure small current (µA) and voltage (mV) changes over a wide range of frequencies (from a few µHz to several kHz). All measurement results need to be sent to a personal computer (PC) for further detailed investigation.

Requirements for the prototype:

- The prototype should have an interface to communicate with a PC in order to receive commands and send the measured data.
- The current and voltage of the investigated battery cell should be measured (24 bit ADC) and stored for further research in battery models.
- For safety reasons the temperature of the battery and the prototype itself should be monitored and a self-shut-down mechanism has to be implemented.
- The prototype should be capable of charging and discharging the investigated battery cell with up to 50 A.
- In order to test battery cells for HEVs and EVs, the prototype should be designed to work in parallel to drive charge and discharge regimes with a multiple of 50 A.

2 Related work

This chapter gives an overview of the principle of batteries. On the one hand, basic information and important definitions are provided. On the other hand, the different behaviour regarding charging characteristics are focussed. To serve as a specific example we will have a closer look at a lead-acid and a lithium-ion cell. Detailed information about all types of batteries and their characteristics are laid out in "Handbook of Batteries" written by Thomas Linden et al[5]. The second part describes how a battery model can be achieved using impedance spectroscopy (IS)[11].

2.1 Batteries

A battery is a device consisting of one or more electrochemical cells that convert their stored chemical energy into electrical energy. This is implicated by an oxidation-reduction process in which electrons are transferred from one to another electrode when the cell is connected to an external load (discharge) or an DC power supply (recharge). The three major components of a cell are the anode (negative electrode), the cathode (positive electrode) and the electrolyte. During an electrochemical reaction the anode on the one side is oxidized and donates electrons to the external circuit. On the otherside the cathode is reduced and accepts electrons from the external circuit.The electrolyte is the ionic conductor and can either be liquid or solid. It is responsible for the transfer of charge (cations and anions) between the anode and cathode inside the cell.

Batteries can be divided into two groups: primary (disposable) batteries and secondary (rechargeable) batteries. Primary batteries are designed to be only used once and discarded, whereas secondary batteries are produced to be used and recharged multiple times. In secondary batteries the chemical process during discharging is reversible. If the voltage at the battery clips is higher than the voltage produced by the normal chemical reaction in the battery, a current in the reverse direction will flow and opposite oxidation takes place.

Table 2.1 shows a comparison of major battery systems in terms of voltage, capacity and specific energy with theoretical and practical values. The maximum energy (theoretical specific energy (Watthours/kilogram)) an electrochemical system can deliver is based on the types (this determines the voltage) and the amount (this determines ampere-hour capacity) of active materials that are used. Due to the need

Table 2.1: Shows different electrode material combinations used in most battery systems. Comparison of the theoretical and the practically achieved characteristics in batteries. [5, page 29]

Battery type	Anode	Cathode	Theoretical values				Practical battery		
			V	g/Ah	Ah/kg	Specific energy Wh/kg	Nominal voltage V	Specific energy Wh/kg	Energy density Wh/l
Primary Batteries									
Alkaline MnO_2	Zn	MnO_2	1.5	4.46	224	358	1.5	145	400
Zinc / air	Zn	Ambient air	1.65	1.22	820	1353	1.5	370	1300
$LiMnO_2$	Li	MnO_2	3.5	3.50	286	1001	3.0	230.	535
Secondary Batteries									
Lead-acid	Pb	PbO_2	2.1	8.32	120	252	2.0	35	70
Nickel-cadmium	Cd	Ni oxide	1.35	5.52	181	244	1.2	35	100
Nickel-metal hydride	MH	Ni oxide	1.35	5.63	178	240	1.2	75	240
Lithium-ion	Li_xC_6	$Li_{(i-x)}CoO_2$	4.1	9.98	100	410	4.1	150	400
Lithium/manganese dioxide	Li	MnO_2	3.5	3.50	286	1001	3.0	120	265
Lithium/iron disulfide	Li(Al)	FeS_2	1.73	3.50	285	493	1.7	180	350

for an electrolyte and for nonreactive components, such as containers, seperators, electrodes, wiring and fuses only a fraction of the theoretical energy of the battery can be practically realized. Another common term to express the output of a battery is the energy density (Watthours /liter) which is the ratio of capacity to volume.

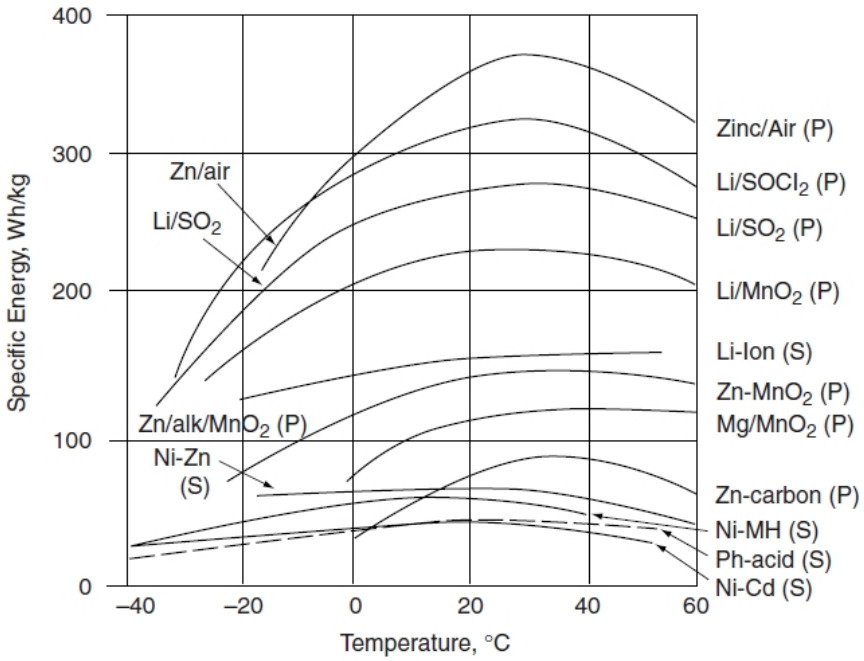

Figure 2.1: Effect of temperature on specific energy of primary (P) and secondary (S) batteries [5, page 153]

The capacity of a battery also changes with the temperature, the load, the age of the battery, how often it was already recharged and deep cycled as well as several other factors. Figure 2.1 serves as an example for the effect of the temperature on the specific energy of some battery systems.

The specific power describes the ratio of the maximum emitable power to the weight, whereas the power density shows the ratio of the maximum emitable power to the volume. This characteristic is a crucial factor for HEVs.

Charging a battery normally includes the charging itself (get the charge into the battery) and the termination (know when to stop charging because the battery is full). A charging scheme is the combination of various charging and termination methods. Every charger and battery manufacturer has its own charging philosophy. Hence, a lot of different charging schemes and parameters exist. [12, 13, 5],

In the following basic charging methods described by Woodbank Communications Ltd, a battery consultancy [13], are shown:

- Constant Voltage
  A constant voltage charger is basically a DC power supply which in its simplest

form may consist of a step down transformer from the mains with a rectifier to provide the DC voltage to charge the battery. Such simple designs are often found in cheap car battery chargers. The lead-acid cells in cars and backup power systems typically use constant voltage chargers. In addition, lithium-ion cells are often charged with constant voltage systems, although these are normally more complex with added circuitry to protect the battery.

- Constant Current
  Constant current chargers vary the voltage they apply to the battery to maintain a constant current flow, switching off when the voltage reaches the level of a full charge. This design is generally used for nickel-cadmium and nickel-metal hydride cells or batteries.
- Taper Current
  A crude unregulated constant voltage source is used for charging. The charge is not a controlled and the current diminishes as the cell voltage builds up. There is a serious danger of damaging the cells through overcharging. In avoidance of overcharging, the charging rate and duration should be limited.
- Pulsed charge
  Pulsed chargers feed the charge current to the battery in pulses. The charging rate (based on the average current) can be precisely controlled by varying the width of the pulses (typically 1 second). During the charging process, short rest periods of 20 to 30 milliseconds between pulses allow the chemical actions in the battery to stabilise by equalising the reaction throughout the bulk of the electrode before recommencing the charge. This enables the chemical reaction to keep pace with the rate of inputting the electrical energy. It is also claimed that this method can reduce unwanted chemical reactions at the electrode surface such as gas formation, crystal growth and passivation. If required, it is also possible to sample the open circuit voltage of the battery during the rest period.
- Burp charging
  Burb charging, also called Reflex or Negative Pulse Charging, is used in conjunction with pulse charging. It applies a very short discharge pulse, typically 2 to 3 times of the desired charging current for 5 milliseconds, during the charging rest period to depolarise the cell. These pulses dislodge any gas bubbles which have built up on the electrodes during fast charging, speeding up the stabilisation process and hence, the overall charging process. The release and diffusion of the gas bubbles is known as "burping". Controversial claims have been made for the improvements in the charge rate and the battery lifetime as well as for the removal of dendrites.
- IUI Charging
  This is a recently developed charging profile used for fast charging of some standard flooded lead-acid batteries from particular manufacturers. Initially, the battery is charged at a constant (I) rate until the cell voltage reaches a

preset value - normally a voltage close to the degassing barrier. This first part of the charging cycle is known as the bulk charge phase. When the preset voltage has been reached, the charger switches into the constant voltage (U) phase and the current drawn by the battery will gradually drop until it reaches another preset level. This second part of the cycle completes the normal charging of the battery at a slowly diminishing rate. Finally, the charger switches again into the constant current mode (I) and the voltage continues to rise up to a new higher preset limit when the charger is switched off. This last phase equalises the charge on the individual cells in the battery to maximise battery life.

- Trickle charge
  Trickle charging is designed to compensate for the self discharge of the battery. Continuous charge is a long term constant current charging for standby use. The charge rate varies according to the frequency of discharge. It is not suitable for some battery chemistries, e.g. NiMH and lithium, which are susceptible to damage from overcharging. In some applications the charger is designed to switch to trickle charging when the battery is fully charged.
- Float charge
  The battery and the load are permanently connected in parallel across the DC charging source and held at a constant voltage below the battery's upper voltage limit. It is used for emergency power back up systems and mainly with lead acid batteries.
- Random charging
  All of the applications explained above, involve controlled charge of the battery. However, there are many applications where the energy to charge the battery is only available, or is delivered, in some random, uncontrolled way. This applies to automotive applications where the energy depends on the engine speed which is continuously changing. The problem is more acute in EV and HEV applications using regenerative braking since this generates large power spikes during braking which the battery must absorb. More friendly applications are in solar panel installations which can only be charged when the sun is shining. They all require special techniques to limit the charging current or voltage to levels which the battery can tolerate.

To scale the charge and discharge current of a battery the C-rate is used. For example, a battery with 1,000 mAh that is discharged at a rate of 1 C should provide a current of 1,000 mA for 1 hour, assuming ideal conditions. The same battery discharging at 2C would deliver a current of 2,000 mA for 30 minutes. A C-rate of 0.5 would provide 500 mA for 2 hours. These common rates are also known as the two-hour discharge (0.5C), the one-hour discharge (1C) and the half-hour discharge (2C).

Lead-Acid Batteries:

Basically, a lead-acid battery consists of an acid-proof housing filled with a 38% sulphuric acid and 62% water. Inside the battery are lead plates (negative electrode) and lead plates with a lead dioxide coat (positive electrode). The caused chemical reaction releases electrons, allowing them to flow as current through an external load. While discharging, the materials of the plates react with the acid and the plates change to lead sulphate. When the battery is recharged, the chemical reaction is reversed. The lead sulphate reforms back into lead and lead dioxide. After the plates are restored to their original condition, the discharge process may be repeated. The nominal voltage of a lead-acid cell is 2 V. The end or cut-off voltage is 1.75 V per cell on a moderate discharge rate. A typical automotive battery, also called SLI battery (starting, lighting, ignition) , consists of six lead-acid cells in series to provide the power for the 12 V board system. Figure 2.2 illustrates the structure of a typical SLI battery used in automotives.

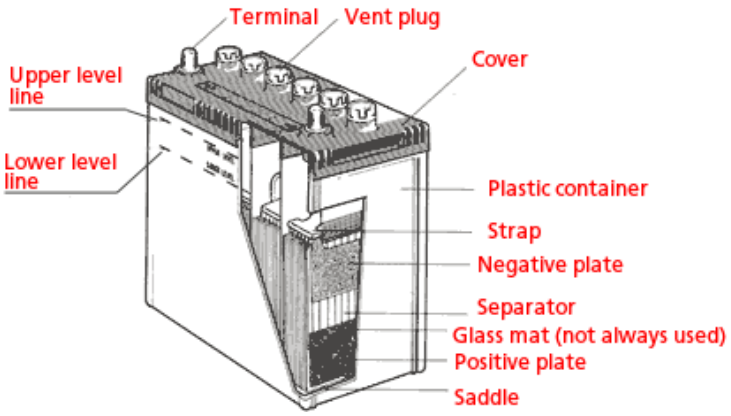

Figure 2.2: Construction of a typical SLI battery [14]

Lead-acid batteries are the oldest and best known rechargeable batteries. They are produced in big quantities differing in shapes and characteristics. As they are already existing for about 100 years, long-term data is available, whereas only estimations exist for e.g. the newer invented lithium-ion cells. Table 2.2 shows the most common types of lead-acid batteries and their typical field of application.

Table 2.2: Types and typical applications of Lead-Acid Batteries

Type	Typical applications
SLI (starting, lighting, ignition)	Automotive, marine, aircraft
Portable	Consumer and instrument applications such as lightning, emergency lightning, radio, alarm systems
Traction	Industrial trucks
Vehicular propulsion	Electric vehicles such as golf carts, hybrid vehicles, mine cars, personnel cariers
Submarine	Submarines
Stationary	Standy emergency power such as telephone exchange, uninterruptible power systems (UPS)

Self Discharge: The self-discharge of a lead-acid cell (open circuit) compared to others is quite rapid. The self-discharge rate depends on several factors such as temperature, acid concentration and the used material for the electrodes in terms of material type and purity. In an open circuit, lead and lead dioxide are reacting with the electrolyte (sulfuric acid) . Lead dioxide reacts to $PbSO_4$, water and oxygen, whereas lead itself reacts to $PbSO_4$ and hydrogen. The higher the acid concentration and the temperature, the higher is the gassing rate. By incorporating a low antimony grid or a calcium-lead grid, the self-discharge rate can significantly be reduced. Figure 2.3 shows such a capacity loss in days and in dependency of the temperature.[5]

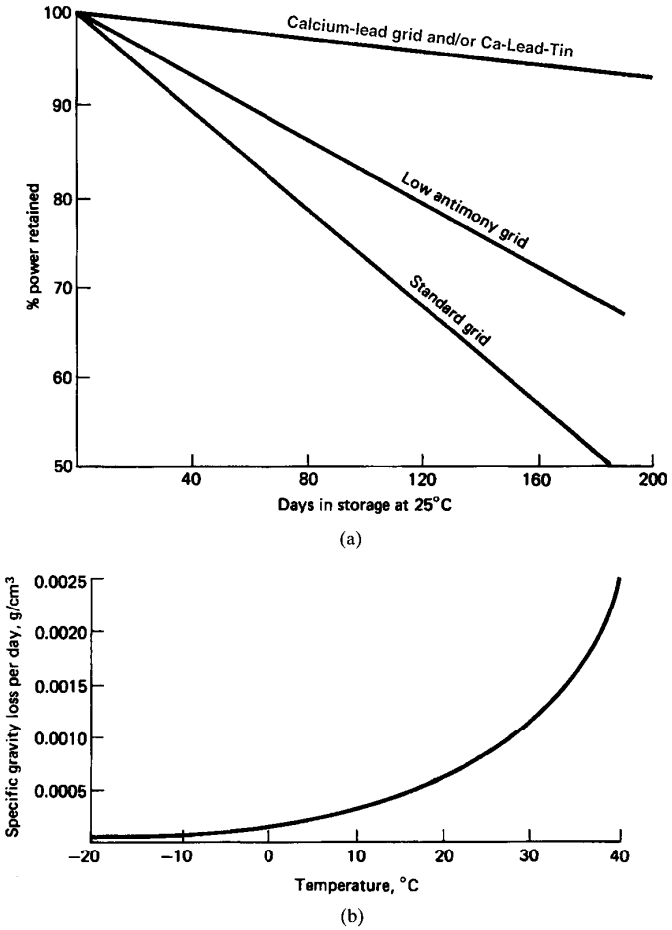

Figure 2.3: (a) Capacity loss during storage or stand at 25°C. [A. Sabatino, Maintenance-free Batteries, Heavy Duty Equipment Maintenance, Irving-Cloud Publishing, Lincolnwood, Ill., 1976.] (b) Loss of specific gravity per day with temperature of a new, fully charged lead-acid battery with low antimonial lead grid. [Special Issue on Lead-Acid Batteries, J. Power Sources 2(1) (1977 / 1978).][5, page 599]

Charging There are a lot of different charging methods for lead-acid batteries. The best method is dependent on the type of battery (used material and physical construction), the available time for charging, service conditions and available charging facilities. In general, a lead-acid battery can be charged at any current rate that does not produce excessive gassing or high temperatures. Low gas production will be recombined within the battery without any problems. At the beginning of charging the battery is able to absorb a quite high current, but the current should be reduced when the battery is fully charged so that the voltage is always just below the gassing voltage.

Lithium-ion batteries:

Lithium-ion batteries are the standard in small consumer devices such as mobile phones, laptop computers and personal digital assistants (PDA). They are also one of the first choices for HEVs and EVs (without considering the current cost factor) because of the high energy density, specific energy and long cycle life they provide. There are a lot of different variations in terms of the used electrode materials and electrolytes. Table 2.3 illustrates the most applicable electrode materials and their theoretical potentials. Because lithium is highly reactive to water, it cannot be used as electrolyte. Therefore, a nonaqueous or aprotic (the hydrogen is bounded tightly to carbon) solution must be used. The electrolyte material can be classified into (1) a liquid electrolyte, which is mostly a lithium salt in an organic solvent, (2) a layer of gel-polymer electrolyte, such as polyethylene oxide or polyacrylonitrite or (3) a layer of solid electrolyte.

Table 2.3: Possible positve and negative electrode materials for lithium-ion batteries.[15]

Electrode material	Average potential difference	Specific capacity	Specific energy
Positive electrodes			
$LiCoO_2$	3.7 V	140 mAh/g	518 Wh/kg
$LiMn_2O_4$	4.0 V	100 mAh/g	400 Wh/kg
$LiNiO_2$	3.5 V	180 mAh/g	630 Wh/kg
$LiFePO_4$	3.3 V	150 mAh/g	495 Wh/kg
Li_2FePO_4F	3.6 V	115 mAh/g	414 Wh/kg
$LiCo_{1/3}Ni_{1/3}Mn_{1/3}O_2$	3.6 V	160 mAh/g	576 Wh/kg
$Li(Li_aNi_xMn_yCo_z)O_2$	4.2 V	220 mAh/g	920 Wh/kg
Negative electrodes			
Graphite (LiC_6)	0.1-0.2 V	372 mAh/g	372-744 Wh/kg
Titanate ($Li_4Ti_5O_{12}$)	1-2 V	160 mAh/g	160-320 Wh/kg
Si ($Li_{4.4}Si$)	0.5-1 V	4212 mAh/g	2106-4212 Wh/kg
Ge ($Li_{4.4}Ge$)	0.7-1.2 V	1624 mAh/g	1137-1949 Wh/kg

Charging: All kind of lithium-ion cells are normally charged with a constant current and constant voltage with a taper charge regime. Figure 2.4 shows such a charging process of a typical lithium-ion battery as it is used in a computer laptop battery. The battery is charged with a constant current until the battery voltage reaches a certain level and from that moment on this voltage is kept constant which leads to a continous reduction of the charge current. This kind of charging regime is also known as CCVC regime .

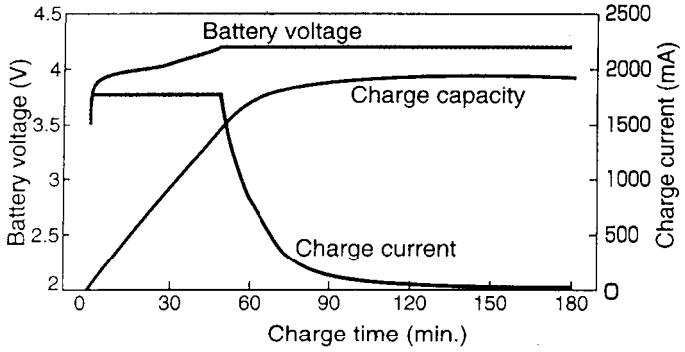

Figure 2.4: Charging characteristics of a typical cylindrical 18650 lithium ion battery at 20°C. Battery is charged at constant current of 1.8 Amps (nominal C-rate) to 4.2 Volts followed by a taper charge at this voltage for a total time of 2 hours.[5, page 485]

2.2 Impedance spectroscopy and battery modelling

In general, impedance spectroscopy (IS) can be described as the small-signal measurement of the linear electrical response of a material of interest over a wide range of frequency. Impedance spectroscopy is also known as dielectric spectroscopy as well as elechtrochemical impedance spectroscopy (EIS). This technique is employed in a wide varity of scienitific fields such as corrosion, batteries, fuel cells, paints, coatings and supercapacitors.

The basic design of a battery is always similar, even so a wide varity of different types and chemistries exists. Every cell consists of a cathode, an anode, an electrolyte and a separator to prevent electric contact between opposite electrodes. Hence, these components have several cell elements and characteristics in common which leads to a similar electrochemical impedance spectrum. Figure 2.5 illustrates a typical IS curve of a lithium battery with its assocciated electrochemical reactions. Nevertheless, it is similar for most batteries. The frequency range of interest is from a few µHz to several kHz.

The electrochemical impedance measuring is normally done by applying an AC voltage to the cell and measuring the occuring current through the cell. Electrochemical cells are not linear. Hence, the applied voltage to the cell must be quite small (in the range of some mV) in order to have a pseudo-linear system.

In terms of rechargeable batteries basically three different measurement methods are used to determine the impedance:

- The current-pulse-method measures the impedance resulting from a step function voltage.
- Imprintation of a time-dependent signal in form of white noise.

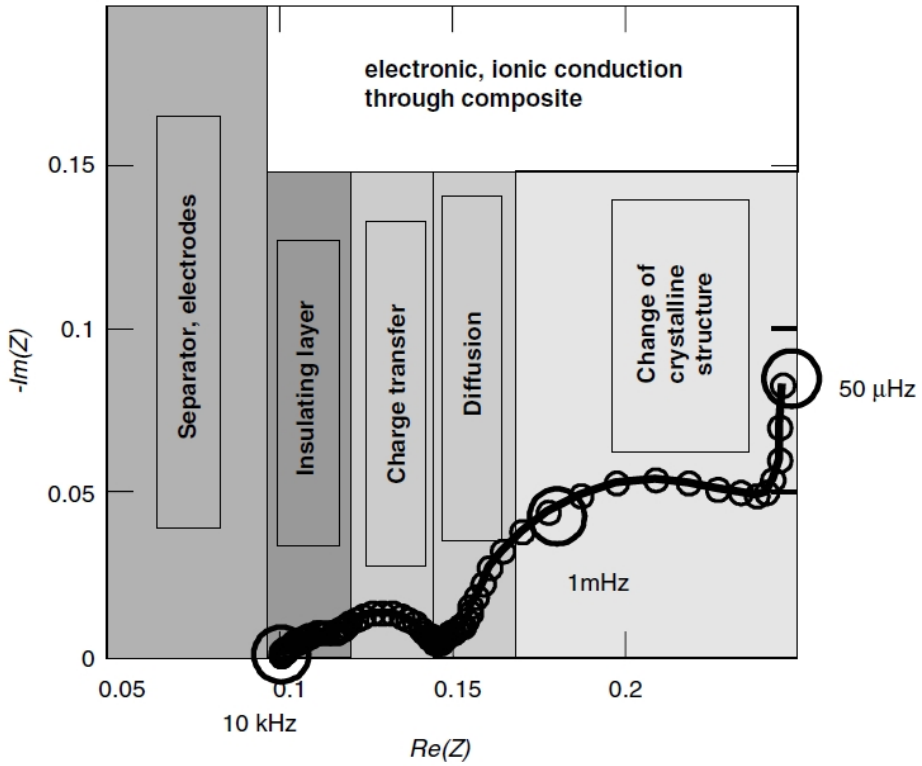

Figure 2.5: Typical IS curve of a lithium-ion battery. [11, page 459]

- The impedance, as a direct frequency-dependent value, is directly determined by using a sinusiodal modulation (at a given frequency).

The most common method of analysing the measured IS data is its fitting into an equivalent circuit model. Such a model mainly consists of common electrical elements such as resistors, inductors and capacitors as well as a few specialized electrochemical elements such as Warburg diffusion elements. Several elements can be combined in both, series and parallel, to build a network that describes the measured IS spectra. The shape of the model's impedance spectrum is controlled by the type of electrical components used in the model and their interconnections. The parameters such as the value of a resistor or capacitor control the size of each feature in the spectrum. Normally, only elements representing a physical or electrochemical reaction of the battery are used. Unfortunately, the analysis of the impedance spectra is complicated by the fact that the impedance at any given frequency usually depends on more than one chemical reaction or physical effect. The most common reactions/effects are listed in following[16, 17]:

- electrolyte resistance
  The electrolyte resistance depends on the ionic concentration, temperature and type of ions.

- double layer capacitance
  A double layer capacitance is formed at the boundary between the electrode and the surrounding electrolyte.
- polarization resistance
  The polarization resistance occurs whenever the potential of an electrode is unequal to their open-circuit potential.
- charge transfer resistance
  The charge transfer resistance is defined by the speed of the redox reaction between the electrode and electrolyte.
- diffusion
  A diffusion is the movement of molecules from a higher to a lower concentration gradient. This can create an impedance called a Warburg impedance.
- coating capacitance
  A coating capacitance is formed when two conducting plates are seperated by a non-conducting media.

Figure 2.6 shows a simple equivalent circuit model of a battery where the charge transfer reaction and the diffusion (Warburg impedance) is incorporated.

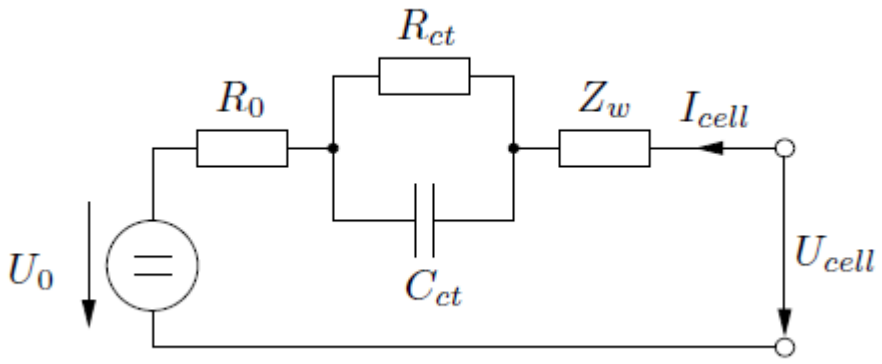

Figure 2.6: Simple equivalent circuit model of a battery. The different components are the idle voltage (U_0), the additional ohmic drop of the cell (R_0), the charge transfer reaction (R_{CT} and C_{CT}) and the Warburg impedance (Z_W).

Further information about the basics in IS can be found in [16] and [17]. Moreover, the practical use of IS to obtain a battery model is reported for instance in [18] and [19].

3 Automated measurement system

This chapter describes the realisation of the prototype. First, the overall idea of the system is explained on the basis of a block diagram. Afterwards, the realised hardware is described. Finally, the developed software for controlling the low distortion power amplifier and the communication with the PC is roughly explained. Additionally, the schematics, the used jumper configuration and a user manual for the possible PC commands are attached in the appendix.

3.1 System overview

The prototype consists of two parts, the low distortion power amplifier itself and a control and measurement unit. The block diagram is shown in figure 3.1. The control system communicates with the PC over USB. The PC (user) sends configuration, start and stop messages to the micro controller (µC) , whereas the micro controller sends back data and info messages. The reference signal for the power amplifier is calculated by the micro controller. Therefore it uses the received set-up data from the PC, the effective voltage and current of the battery and five temperature sensor signals. Four temperature sensors can be placed at different positions right next to the battery cell and one sensor is fixed at the heat sink of the amplifier unit. The power amplifier then converts and amplifies the voltage reference signal, in the range from -5 V to + 5 V, to a reference current, which equals to -50 A to +50 A. Hence, 1 V equals to 10 A current through the battery. A power source with ±12 V and +5 V supplies the system, whereby the 5 V are used for charging and discharging the battery. The ±12 V are used for driving the operational amplifiers (OPA) and the whole control unit.

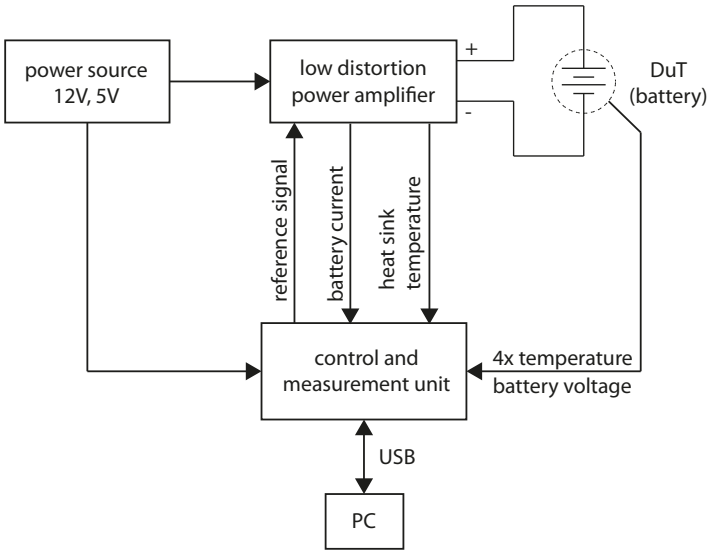

Figure 3.1: System overview of the realised prototype. The PC (user) communicates with the control unit, which drives the amplifier, which again charges or discharges the battery.

3.2 Low distortion power amplifier

This section describes the realisation of the power amplifier stage. First, the basic function is described on the basis of the block diagram. The following subsections discuss each part of the block diagram in detail. Finally, an overall simulation in LT-Spice of a single amplifier stage is explained.

Walter Meusburger presents in his Ph.D. thesis "A Novel Power Amplifier Topology without Crossover Distortion" [20] a power amplifier topology with the efficiency of a class B amplifier, where the crossover distortion is completely avoided. Additionally, there is even no necessarity for component trimming. Furthermore, a comparison to other topologies are shown. With the input of these ideas among others, we developed the below explained low distortion power amplifier.

Figure 3.2 shows the block diagram. A reference input signal in the range of -5 V to +5 V is compared with the measured signal by an integrating controller. Then the signal is split into the positive and negative part. Further, each signal gets conditioned to drive the p-stage and n-stage with its power PMOS and NMOS. The positive stage is a voltage controlled current source and the negative stage is voltage controlled current sink. Depending on the state of the stages the attached battery gets charged or discharged. The charge/discharge current is measured by means of a current transducer and further transformed to a voltage signal (10 A is equivalent

to 1 V). This signal then serves the control loop.

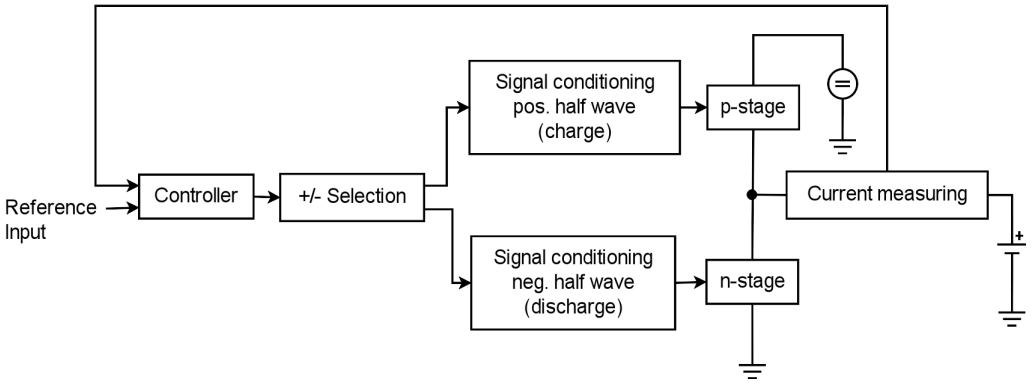

Figure 3.2: Basic block diagram of the low distortion power amplifier.

Because of the desired 50 A charge and discharge current and the resulting heat losses, the amplifier printed circuit board (PCB) consists of four identically constructed amplifier pairs. Hence, each pair is capable of 12.5 A.

Figure 3.3 illustrates the prototype layout and its sectioning. The size of the printed circuit board is 160 mm x 100 mm. The power components are mounted on a big common heat sink on the bottom side. The whole power supply and measurement are done through a 64 pole jack. The battery is connected to the plugs on the left side. The switch at the bottom right opens and closes the control loop of the superior current controller. When the amplifier is used in combination with the control unit, the switch is replaced by an analog switch which is controlled by the micro controller of the control unit.

The overall layout attention is already turned on the idea of using multiple amplifiers in parallel for higher currents. This could be easily implemented into a standard 19" rack.

3.2.1 +/- selector

This block splits the signal into its positive and negative part. Furthermore, a small constant voltage is added in the time where it would be zero in order to keep a quiescent current through the transistors. This is done by a simple diode network. Figure 3.4 shows the circuit and waveform of the +/- selector whereat V_{stell} is the input signal, V_{stell-} the negative half wave and V_{stell+} the positive half wave. Since there is no exactly defined quiescent current necessary, resistors (R1, R2, R3, R4) are used as current source and current sink instead of an high accurate solution. Diodes D1-D3 generate the negative signal and diodes D4-D6 the positive signal [21]. Resistor R5 and R6 set the quiescent current to around 240 mA per transistor.

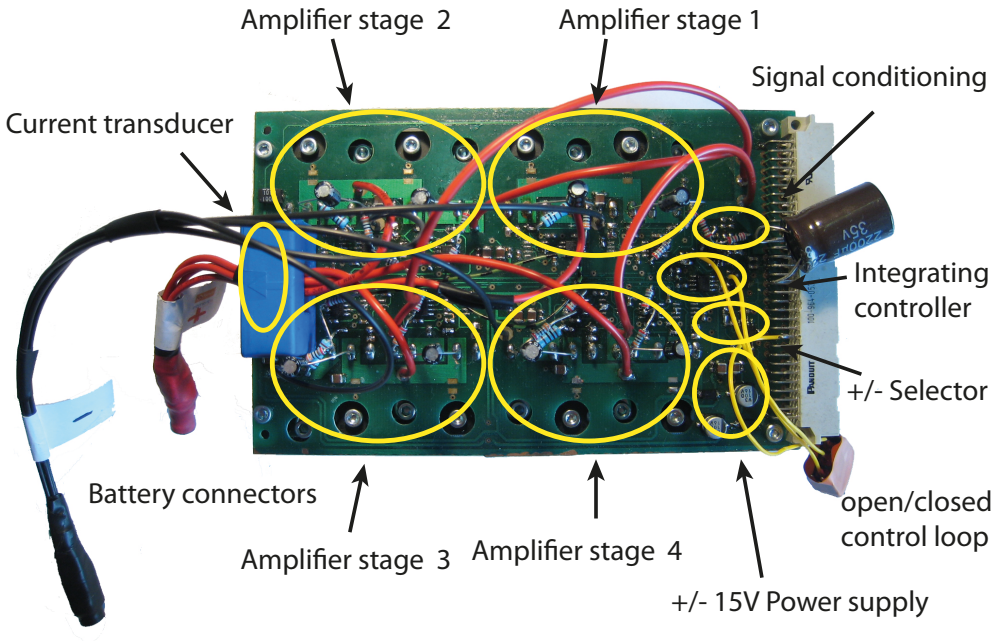

Figure 3.3: Principle layout on the printed circuit board.

3.2.2 Signal processing for the positive stage

The positive signal from the +/- selector is related to the ground and has to be subtracted from the 5 V supply voltage in order to be related to the supply voltage to drive the hi-side PMOS. Figure 3.5 displays the used circuit and the gained waveforms whereas V_{stell+} is the input signal and $V_{stell++}$ is the output signal.

Tests with the first prototype showed that it is better to keep the driving signal as big as possible to minimize parasitic errors. The driving signal then gets weakened to its necessary small size as late as possible. Therefore, the voltage divider with R13 and R14 is implemented four times directly before the input of the following OPA of the p-stage.

3.2.3 Signal processing for the negative stage

The situation is similar with the negative signal V_{stell-}. But the signal is already related to the right potential and only has to be inverted. Figure 3.6 shows the used circuit and the gained waveforms whereat V_{stell-} is the input signal and $V_{stell--}$ is the output signal. Again, the driving signal gets weakened to its necessary small size as late as possible. Hence, the voltage divider with R3 and R4 is implemented four times directly before the input of the following OPA of the n-stage.

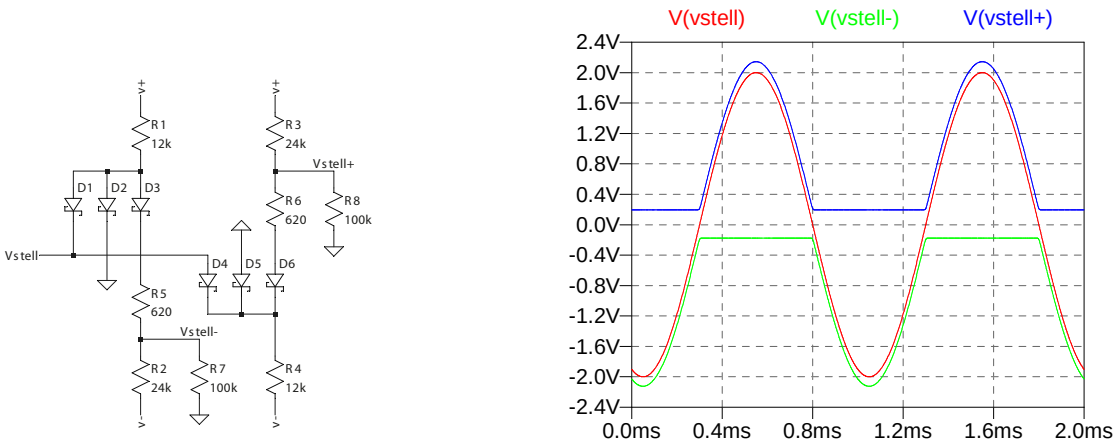

Figure 3.4: Circuit (left) and signal curve (right) of the +/- selector.

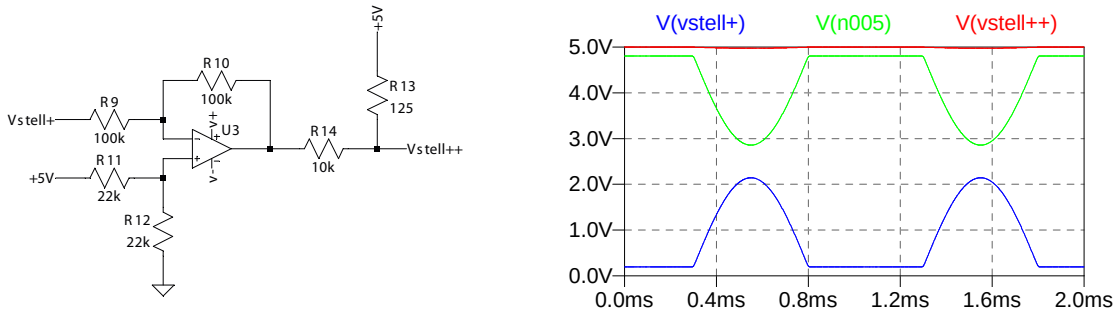

Figure 3.5: Circuit (left) and signal curve (right) of the positive signal processing.

3.2.4 Negative stage - voltage controlled current sink

In figure 3.7 the circuit of one of four identically build closed loop controlled n-stages is shown. The voltage across resistor R5 [22] is compared with the input signal $V_{stell--}$. The low pass filter consisting of capacitor C1 and resistor R6 limits the slew rate of the operational amplifier to avoid oscillations at frequencies lower 20 kHz. [23]

The two components R8 (output resistance of the operational amplifier) and C2 (source gate capacitance of the n-mosfet) were only used in the simulation to terminate a rough value for C1. Simulations resulted in 3 nF for C1 but measurements with the prototype showed that 1 nF is already enough.

3.2.5 Positive stage - voltage controlled current source

Figure 3.8 shows the circuit of one of four identically build closed loop controlled p-stages. By analogy with the n-stage, the voltage across resistor R16 [22] is compared with the input signal $V_{stell++}$. The low pass filter consisting of capacitor C3 and

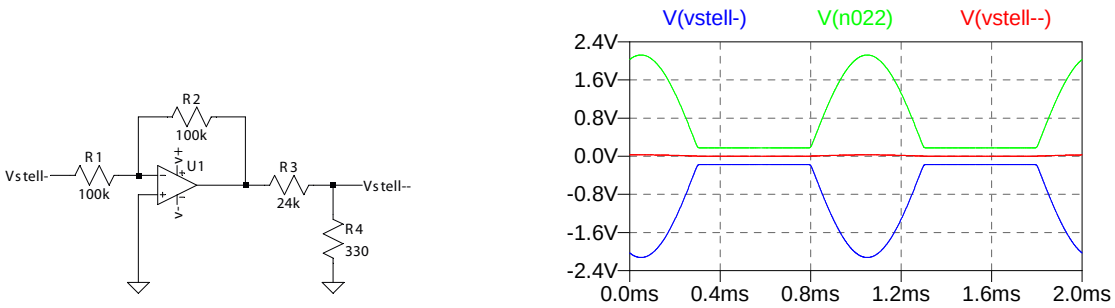

Figure 3.6: Circuit (left) and signal curve (right) of the negative signal processing.

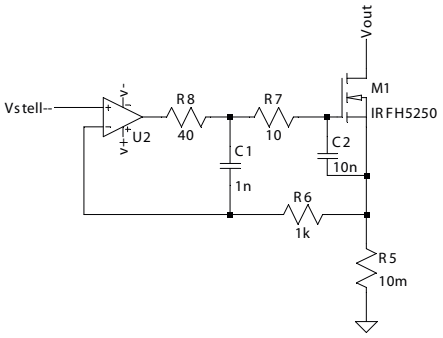

Figure 3.7: Circuit of the closed loop controlled n-stage.

resistor R15 limits the slew rate of the operational amplifier to avoid oscillations at frequencies lower 20 kHz. [23]

The two components R18 (output resistance of the operational amplifier) and C4 (source gate capacitance of the p-mosfet) were only used in simulation to terminate a rough value for C3. Simulations resulted in 3 nF for C3 but measurements with the prototype showed that 1nF is already enough.

3.2.6 PI controller

To minimize the control error of the four individual stages, a second overall PI-controller is implemented that compares the measured current with the reference signal. The controller can be switched on and off by software with an configuration message. In general, it is better to use the controller for low frequencies (lower 1 kHz). Further information about the use of the controller is given in section 4.1 experiments and measurements.

The values of the PI-controller are determined on an empirical basis. Hence, there is potential for optimization.

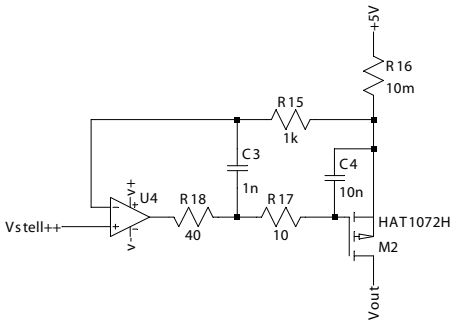

Figure 3.8: Circuit of the closed loop controlled p-stage.

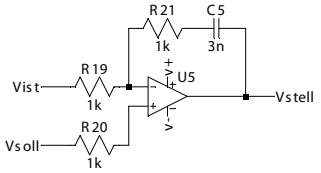

Figure 3.9: Circuit of the PI-controller.

3.2.7 Overall simulation of a single stage

The combination of all single parts leads to the overall simulation, which is shown in figure 3.10. For reasons of clarity and comprehensibility only a single stage is shown. The voltage divider ratio R29/R30 and R15/R27 is by the factor of four too small and instead of the desired 50 A only 12.5 A will be possible.

The current transducer LEM LA55-P is simulated by the resistors RS1 and R11, the capacity C4 and a voltage controlled voltage source E1.

An easy battery model consisting of the resistor R3 and R4, the capacity C1, the inductance L1 and a voltage source V3 serves as battery. Changing the values of L1 simulates different length of connection cables.

The inductance of leads from the battery to the amplifier and the capacitive behaviour of the battery create an oscillator . To eliminate this upcoming oscillations a low pass filter is implemented in the power path between the current source and current sink of the amplifier.

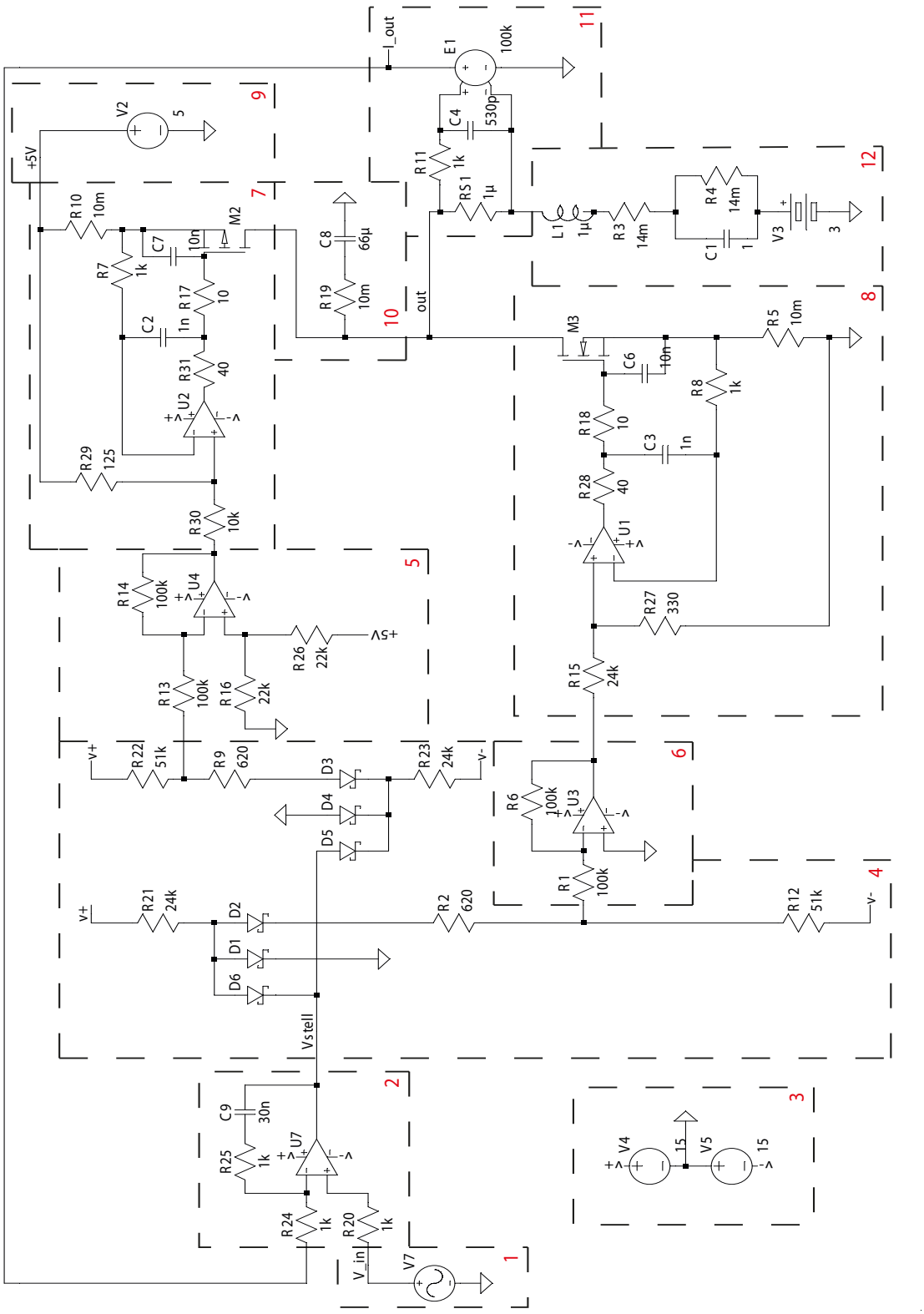

Figure 3.10: Overall simulation of a single stage. (1) signal generator for input signal (2) overall integrated controller (3) power supply for operational amplifiers (4) positive / negative signal selector (5) positive signal conditioning (6) negative signal conditioning (7) positve amplifier (8) negative amplifier (9) +5 V power supply (10) lowpass filter (11) current transducer (12) battery model.

3.3 Description and hardware realisation of the control and measurement unit

Figure 3.11 shows the basic idea of the control and measurement unit. The core is a STM32F103 micro controller. It communicates bidirectionally with the PC through USB and stores and obeys the received commands. Further, it calculates the values for the power amplifier. The generation of the voltage reference signal for the power amplifier is done by an PCM1794 digital-to-analog converter. The data are then transmitted via PCM Audio Serial Port Interface in I²S mode to the micro controller. The voltage and current of the battery is measured by an external PCM4222 analog-to-digital converter and the used data transfer is the same as the one used with PCM1794. The five LM335 temperature sensors are connected to the internal ADC of the micro controller. Furthermore, four LEDs for status display and an analog switch to enable and disable the PI-controller of the power amplifier are connected to the micro controller. The whole circuitry is powered by ± 15 V for the operational amplifiers, 5 V for the temperature sensors and USB and 3.3 V for the micro controller, the PCM4222 and the PCM1794.

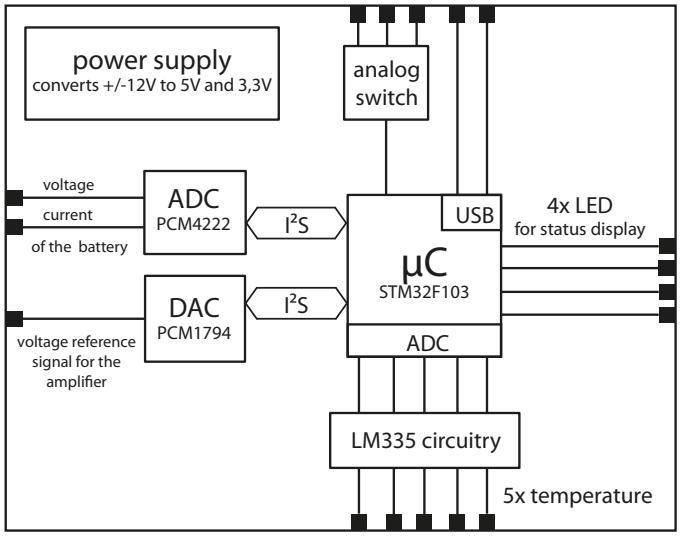

Figure 3.11: Overview of the control and measurement unit.

3.3.1 Battery voltage and current measurement with ADC - PCM4222

The battery current is measured with a current transducer LEM LA55-P[24]. The conversion ratio of 1:1000 combined with a 100 Ωshunt [25] transforms a current of 1 A into 0.1 V. Respectively, a maximum battery current of ± 50 A equals a maximum voltage range from -5 V to +5 V.

The battery voltage is measured directly at the battery clip with the same maximum voltage range from -5 V to +5 V as the current measurement. Hence, the same pre-amplifier circuitry is used.

A PCM4222 [26] is used as analog-to-digital converter. It is a high-performance, two channel, 24bit, 216kHz sampling multi-bit delta sigma analog-to-digital converter. It has differential voltage inputs and a PCM Audio Serial Port Interface. Figure 3.12 illustrates the used signal conditioning circuit. It consists of a fully differential amplifier to adjust the ground based signal to a differential signal. Furthermore, a two-pole low pass anti-alias filter is implemented. The following equations show the complete transfer function whereas first the input differential voltage (V_{id}) and second the output differential voltage (V_{od}) are defined. The first pole of the low pass filter is done by adding capacitors (C14, C15) in the feedback loop. The second pole is created by placing a first order low pass filter at the output of the amplifier (R31 and C16, R53 and C48) as shown in figure 3.12.[27]

$$V_{id} = (V_{in+}) - (V_{in-})$$

$$V_{od} = (V_{out+}) - (V_{out-})$$

$$\frac{V_{od}}{V_{id}} = \frac{Rf}{Rg} \times \frac{1}{1+j2\pi f(RfCf)} \times \frac{1}{1+j2\pi f \times 2 \times RoCo}$$

Since the common-mode voltage outputs of the PCM4222 have a limited drive capability, an operational amplifier OPA227 [28] is used as buffer.

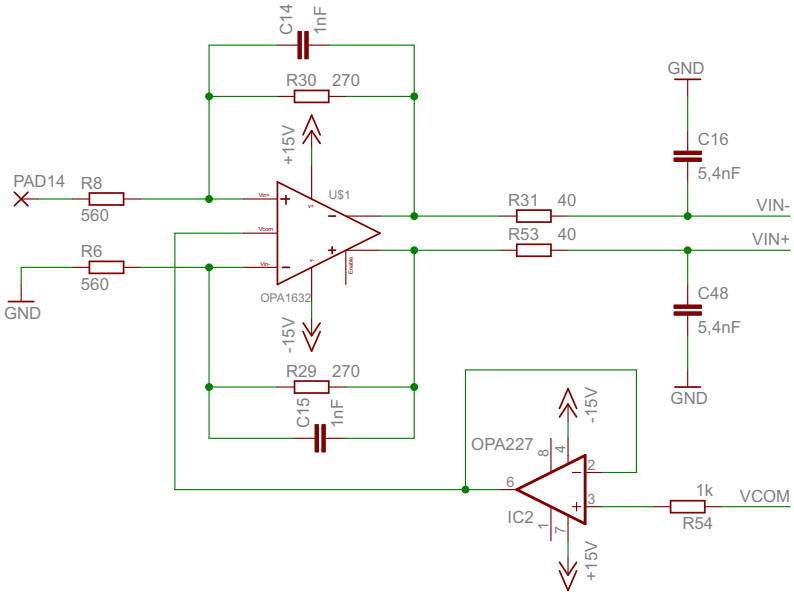

Figure 3.12: Signal conditioning circuit for ADC - PCM4222.

3.3.2 Signal generation for power amplifier with DAC - PCM1794

To generate the desired voltage reference signal from -5 V to +5 V for the power amplifier a PCM1794 [29] is used. This PCM1794 is a 24-bit, 192 kHz sampling, digital-to-analog converter that communicates with the µC over an 3-wire serial port interface. Figure 3.13 displays the needed external standard circuitry in order to obtain the desired high signal to noise ratio of 129 dB. The PCM1794 voltage outputs are followed by differential amplifier stages, which sum the differential signals for each channel, creating a single-ended I/V op-amp output. In addition, the differential amplifiers provide a low-pass filter function. The voltage output level of the I/V converter (V_i) is given by following equation, whereas R_f is the feedback resistance of the I/V converter:

$$Vi = 7.8\,mA_{pp} \times R_f$$

The equation for the difference amplifier with the special case of all resistors with the same value is:

$$V_O = V_{i+} - V_{i-}$$

Hence, with a resistor of 750 Ω each for the feedback gives a voltage output level of 5.85 V for each channel (positive and negative). Combined with the difference amplifier, the single ended output voltage range is from -5.85 V to +5.85 V.

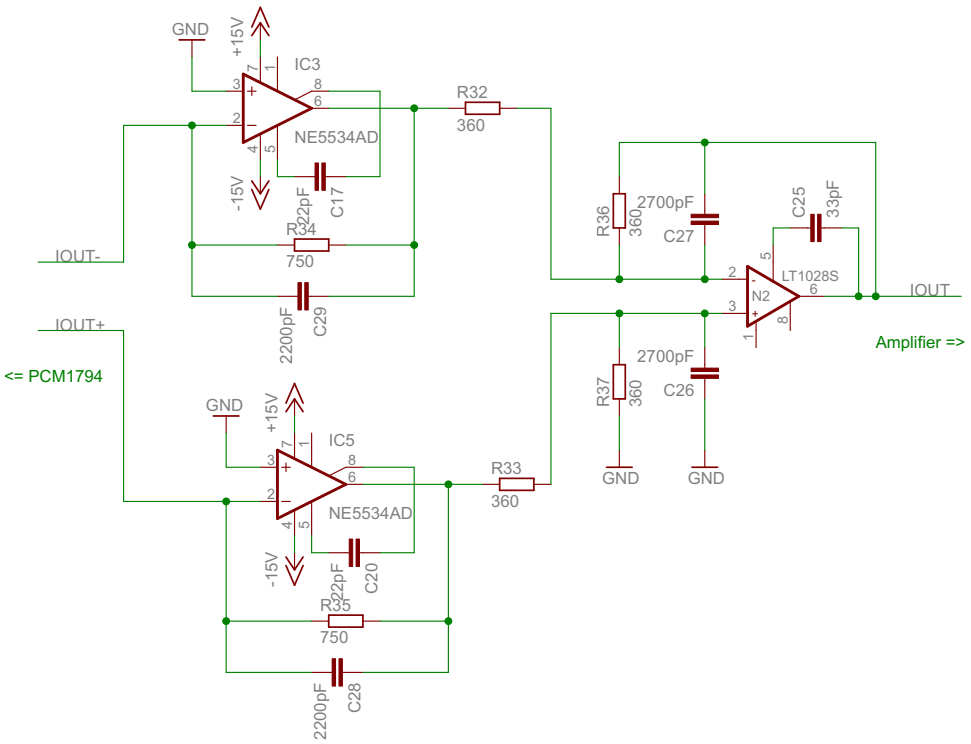

Figure 3.13: Signal generation circuit for amplifier with DAC - PCM1794.

3.3.3 Temperature measurement with LM335

The prototype has a total of five LM335 temperature sensors [30]. One is attached to the heat-sink of the low distortion power amplifier. The other four sensors are utilised for flexible usage to measure the temperature of the battery cell directly at the cell. Figure 3.14 shows the used external circuitry for one sensor. The resistor R14 is used to limit the current through the LM335 sensor. The voltage divider of R15 and R16 adjusts the voltage level to the micro controller level of 3.3 V. The low pass filter of R15 and C9 reduces the high frequent errors. [31]

3.4 Software implementation

The developed software for the STM32F103 µC is written in the programming language “C”. Ride7 from Raisonance was used as software development environment.

Figure 3.15 depicts a basic overview of the implemented software. When the power is switched on, the µC configures itself and all peripheral equipment and establishes the USB connection to the PC. Afterwards, the control unit is ready and is waiting

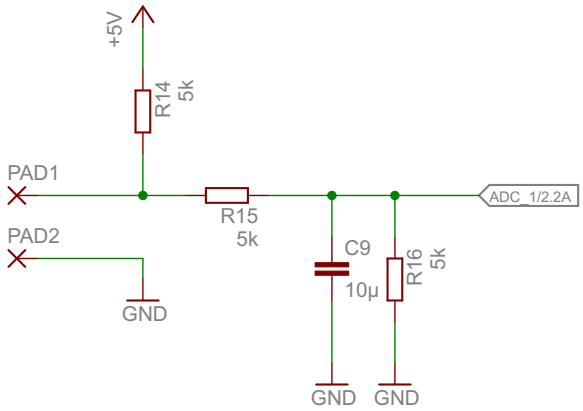

Figure 3.14: Circuit of the temperature measurement (for one temperature sensor).

(in the WAIT state) for the software set-up, done by the user at the PC. The user can now send a list of configuration messages to load a charge / discharge regime for the attached battery. After correct set up the user sends a start message and the first command will be processed. The µC will jump back into the wait state after finishing all commands, the user sends a stop message or a failure occurrs.

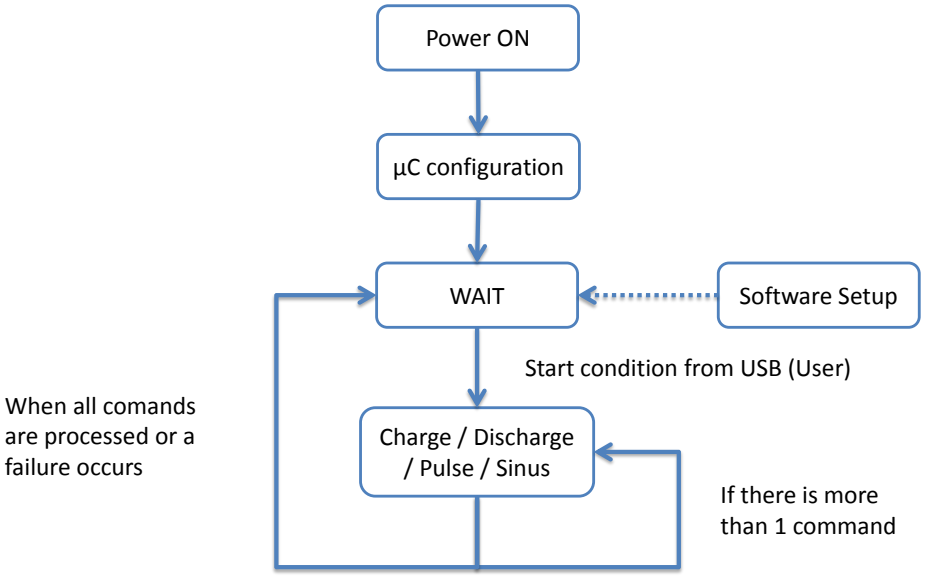

Figure 3.15: Simple flow chart of the implemented software.

After the µC is configured and the USB connection is established, the endless loop of the main program begins. First the WAIT - state is checked. If the WAIT - state is active, do nothing, otherwise the following sequence is executed:

1. Calculate the reference signal for the amplifier.
2. Check if an error (temperature, battery voltage or current) occurred. If so, stop the amplifier and send an error message.
3. Prepare the data message.
4. Store the data message in the USB-buffer in order to send it to the PC.

The main program gets periodically interrupted by the DMA controllers (to process the temperature signals, the battery voltage and current signal) and a timer/counter for timing purpose and none-periodically by the USB interface.
The temperature is measured by a LM335 temperature sensor and is being converted from analog to digital by the internal ADC (ADC1). Afterwards, the data is stored in the internal memory, using the Direct Memory Access (DMA) controller (DMA1). The battery voltage and current are converted from analog to digital by the external ADC PCM4222 and are transferred to the µC via audio serial interface in I^2S mode. The data is then stored in the internal memory using the DMA controller (DMA2). The calculated signal for the amplifier is converted from digital to analog by the external DAC PCM1794. The data to the DAC is sent via an audio serial interface in I^2S mode. To fill the send buffer continuously, the DMA controller (DMA1) is used.

Table 3.1 lists the used interrupts and shows a short description of their usage. The interrupts are priority ranked, which is configured in the NVIC priority group. [32, page 189ff]

Table 3.1: Description and priority order of the used interrupts. (1 is the highest priority)

Priority	Name	Description
1	TIM2_IRQn	Timer 2 is used for all time based actions. (counts every 100µs)
2	DMA2_Channel2_IRQn	Handles the data transfer (DMA2 for the I2S3) of the PCM1794.
3	DMA1_Channel4_IRQn	Handles the data transfer (DMA1 for the I2S2) of the PCM4222.
4	USB_LP_CAN1_RX0_IRQn	Handles the USB communication. (send and receive)
5	DMA1_Channel1_IRQn	Stores the converted temperature data. (ADC1)

3.4.1 USB

The STM32F103RCT has an USB device peripheral integrated which is compatible with the USB full-speed 12 Mb and has software-configurable endpoint setting and suspend/resume support [32, page 599ff]. STM also provides an USB function library to ease the implementation. In our application an USB connection between the µC and a PC is used to establish a virtual RS232 interface. Therefore two endpoints are used. One is for communication and the other one for data transfer. At the PC side a VirtualCOM driver has to be installed. To communicate with the µC, a simple terminal program like HTerm is necessary. [33, 34]

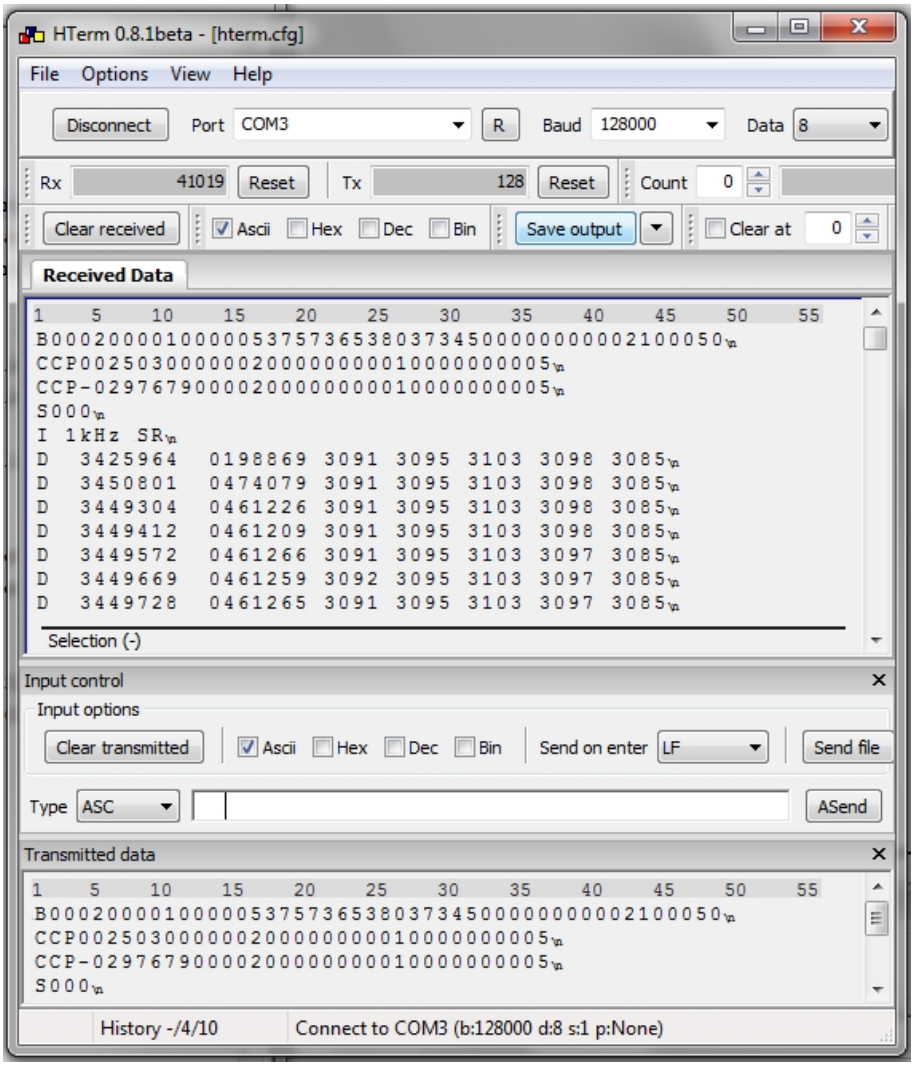

Figure 3.16: Terminal program HTerm used for communication between the control unit and the PC.

Figure 3.16 shows an example how the communication between the control unit and the PC/user could look like. Every transmitted data/command is reapeted by the

micro controller. The first command is a Basic-Confguration-Message to define the sample rate, the battery voltage and current limits as well as the temperature limits. The second line is a Configuration-Message to define a positive pulse, whereas the third line defines a negative pulse. The forth line contains the Start-Message. From that moment on, the control unit sends an Information-Message with the current sample rate (1kHz) followed by the Data-Messages (every millisecond), containing the battery current and voltage and the five temperatures, until the end of the configured program has been reached.

3.4.2 Use of circular buffers in combination with DMA for PCM4222, PCM1794 and the internal ADC for the temperature sensors

To release pressure from the CPU the DMA controllers of the µC are used for continuous data storage of the temperature, the measured battery voltage and the measured battery current. Furthermore, the DMA controller is used to fill the send buffer for the reference signal of the low distortion power amplifier.

The STM32F103 has in total two DMA controllers with 12 possible channels (7 for DMA1 and 5 for DMA2). Both controllers are able to manage memory-to-memory, peripheral-to-memory and memory-to-peripheral transfers. Moreover, the two DMA controllers support a circular buffer management and can be used with the main peripherals (SPI, I2C, USART, general-purpose, TIMx, DAC, I2S, SDIO, and ADC). [32, page 263ff]

Figure 3.17 illustrates the three circular buffers used in our application and their functionality.
(a) shows the circular buffer for the five measured temperature signals. The ADC1 converts continuously and rotatory the five temperature signals. Each time a conversion is finished, a DMA request is done by the ADC1. While the next temperature channel is converted, the DMA controller stores the previous one in the circular buffer. The buffer has a size of 50 entries (10 times each temperature channel).When the buffer is half full the Half Transfer (HT) interrupt flag is set and the DMA IRQ Handler is called. In that interrupt service routine the mean of the lower half buffer (five values for each of the five temperature channels) is calculated while the DMA controller stores the next temperature values in the upper half of the circular buffer. When the DMA controller reaches the last entry of the buffer the Full Transfer (FT) interrupt flag is set and again the associated DMA IRQ Handler is called. This time the mean of the upper half is calculated while the next temperature values are already stored in the lower half of the buffer.
(b) shows the circular buffer for the battery voltage and current measurement. The external ADC PCM4222 converts the current and voltage signal continuously and

sends them via I²S channel (I2S2) to the µC. The I²S protocol [35] only allows the transfer of 16bit data packages, but the PCM4222 converts with a accuracy of 24bit. Hence, two data packages are sent to transfer the 24 bits. The PCM4222 sends continuously and alternately the two data packages for the first channel (current) and then the two data packages for the second channel (voltage). Each time, a data package is stored in the receive buffer of the I²S interface, a DMA request is sent and the DMA controller transfers the data package to the associated circular buffer. During the DMA controller fills the upper half of the buffer, the CPU merges the two current and voltage data packages from the lower half into valid numbers and stores it at another place. The same process is respectively done with the upper half of the buffer when the Transfer Complete (TC) interrupt is set.
(c) shows the circular buffer for the amplifier reference signal. The external DAC PCM1794 needs a 24bit number to generate the analog amplifier reference signal. Hence, the number has to be split up into two 16bit packages in order to transmit them via I²S protocol. The DMA controller fills the send buffer continuously with values from the circular buffer and sets alternately the Half Transfer and Transfer Complete interrupt flag. Each time an interrupt occurs, the CPU calculates the next value for the amplifier reference signal and stores it in the circular buffer.
The Transfer Error (TE) interrupt flag is set when the CPU and the DMA try to read/write at the same address at the same time.[32, page 269]
In our application the error flag is reset and an error message is sent that either the measured data is corrupted or the amplifier reference signal is wrong.

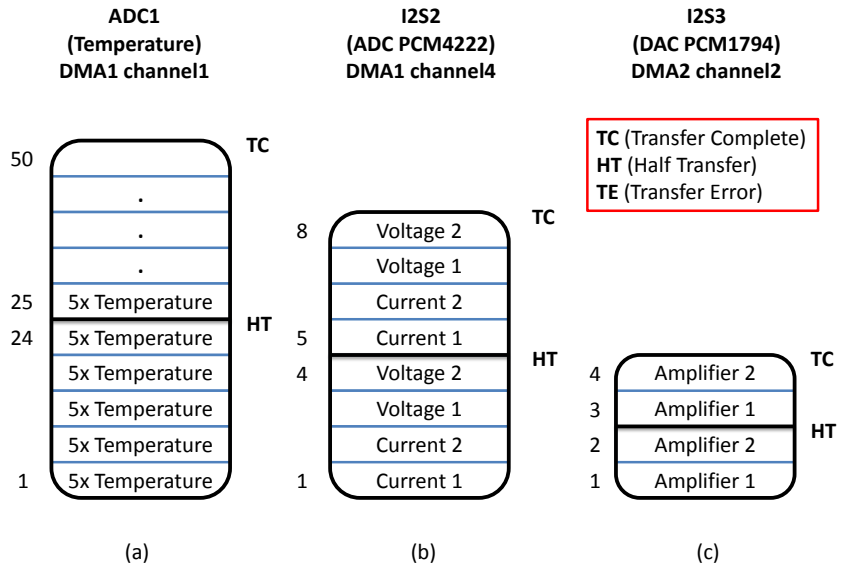

Figure 3.17: Use of the DMA controllers to manage the data with circular buffers from (a) the 5 temperature signals, (b) the measured voltage and current signal of the battery and (c) the amplifier reference signal.

3.4.3 Messages & modes

The communication between the µC and the PC via an terminal program is done by so called messages. Each message has a maximum size of 64 bytes. The messages are written in plain text, so the 64 bytes is equal to 64 characters. The first character is always used as identifier to recognize the type of message. The following list shows the possible messages and the associated identifier character in brackets:

- Start message (S)
  It's the start command the user has to send in order to start the configured charge / discharge regime.
- Stop message (H)
  With this message the user can stop the running charge / discharge regime with some possible options.
- Basic-Configuration message (B)
  Fundamental settings such as temperature, voltage and current limits, offsets and sample rate steps are adjusted with this message.
- Configuration message (C)
  The µC can store a maximum of 200 Configuration messages to build a charge / discharge regime described in section 2.1. The options CCVC charging and discharging, pulse charging and discharging as well as sine wave forms are implemented so far. The charging regimes can be easily extended by adopting the software of the micro controller.
- Error message (E)
  If one of the configured limits is exceeded, an error message is sent to the user.
- Information message (I)
  Information messages are sent to the user to indicate that the system is ready or a new configuration message is processed.
- Data message (D)
  A data message consists of the five temperature values, the battery voltage and the battery current. The transmission rate is defined in the basic configuration.

A configuration message always consists of a message prefix 'C', followed by an 'O' for open or a 'C' for closed loop (use of PI-controller). The third character indicates the operating mode Pulse 'P', Sinus 'S', Charge 'C' or Discharge 'D'. The rest of the configuration message depends on the operating mode:

- Pulse
  The pulse is defined by the desired battery current (in mA), the on-time (in ms), off-time (in ms) and the number of repetitions.

- Sinus
  The sinus is defined by the desired battery current amplitude (in mA), the frequency (in µHz) and the number or repetitions.
- Charge
  The charging is a CCVC regime. Firstly, it is charged at a constant current (in mA) to a defined voltage (in mV), followed by a taper charge at this voltage until the defined end current (in mA) is reached. From that moment on the end time counter (in ms) runs and the charging at the defined voltage is finished when the counter stops.
- Discharge
  The discharging is a CCVC regime. Firstly, it is discharged at a constant current (in mA) down to a defined voltage (in mV), followed by a taper discharge at this voltage until the defined end current (in mA) is reached. From that moment on the end time counter (in ms) runs and the discharging at the defined voltage is finished when the counter stops.

In the appendix, figure 5.11 and figure 5.12 explain the messages and their possible entries in more detail.

4 Experiments & measurements

This chapter is concerned with experiments and measurements to characterise the performance of the prototype.
First, the low distortion power amplifier itself will be described. Next, the experiment is done with the overall system. Furthermore, a measurement with a real battery cell of A123 Systems is done to show the idea of impedance spectroscopy investigations. Finally, some suggestions for the improvement of the prototype are presented.

4.1 Low distortion power amplifier

While writing this thesis, parts of the measurements done in this section have already been published in the paper "Low Distortion Power Amplifier for Battery Measurement Systems" [36] and are described in the current thesis for the sake of completeness.

Measurement setup

Figure 4.1 shows the used measurement set-up. Two programmable four channel high-performance power supplies HMP4040 [37] from HAMEG Instruments are used to power the system (for the 5 V, 50 A as well for $\pm$15 V). For the generation of the amplifier reference signal an arbitrary function generator HMF2550 [38] from HAMEG Instruments is used. The measurement was done by a 350 MHz / 4 GSa / 4 MB digital oscilloscope HMO3524 [39] from HAMEG Instruments.

Neither a temperature nor a voltage and current monitoring is implemented in the power amplifier. Due to the lack of implemented safety features three in series connected super caps (a 2.7 V, 2400 F) serve as device under test. In case of a short circuit, a 70 A fuse is integrated in the power path between the amplifier and the battery. Further, an external radial cooler is used to keep the temperature of the power amplifier at a low level.

Measurements

The length of the transient response depends on the type of battery and the state of charge (SOC). Experiments with different cells and SOC showed an average length

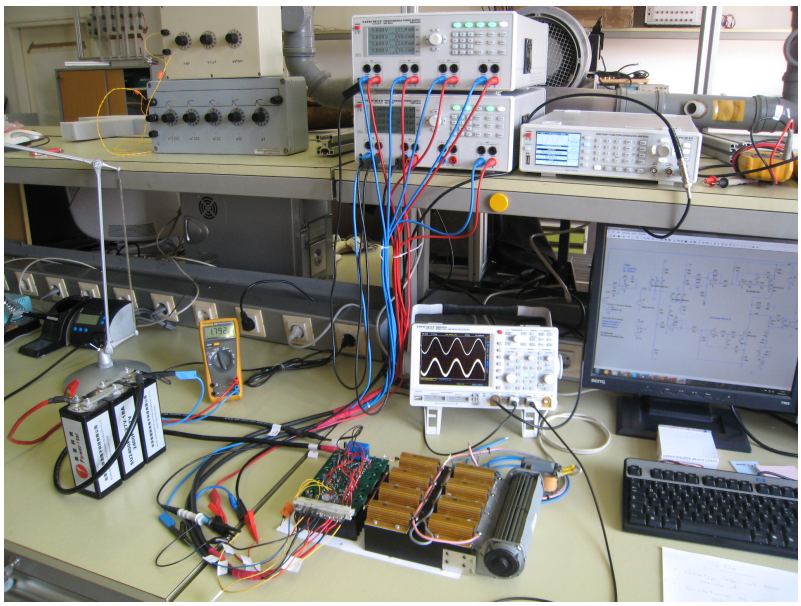

Figure 4.1: Measurement setup to verify the capability of the low distortion power amplifier prototype.

of about 200 µs. Figure 4.2 displays the transient response to a 5 V_{pp} rectangular reference input signal.

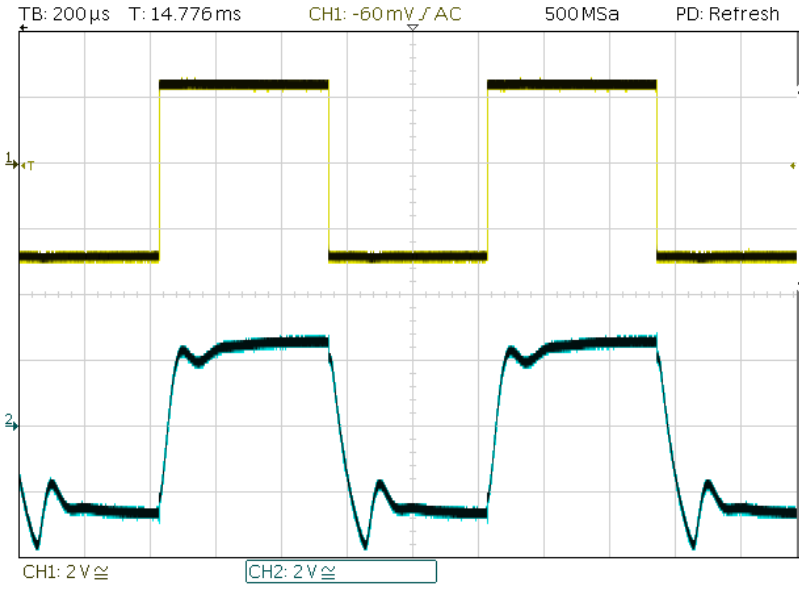

Figure 4.2: Rectangular reference input signal, Vpp=5 V, f=1 kHz [upper]; measured signal [lower].

The reaction of the amplifier to the reference signal for low frequencies the amplifier meet the expectations. For example, a reference triangular input signal with a peak-

to-peak voltage of 5 V (equal to ±25 A at the output) at a frequency of 50 Hz is compared to the transduced output signal in figure 4.3.

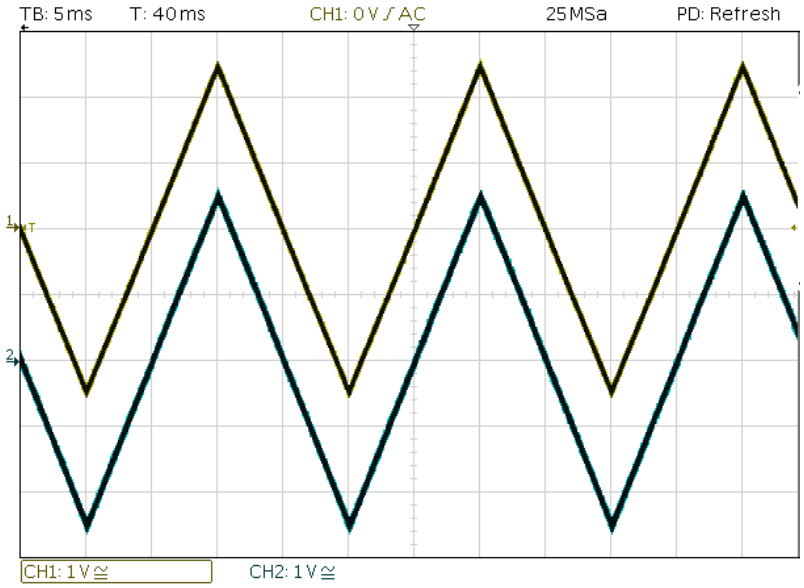

Figure 4.3: Triangular reference input signal, Vpp=5 V, f=50 Hz [upper]; measured signal [lower].

At frequencies greater than 1 kHz the inductance of leads is getting dominant. In order to drive higher currents the easiest options are to reduce the length of leads or to increase the power supply voltage. Figure 4.4 shows two sinus signals with 5 V peak-to-peak at a frequency of 18 kHz, one using the overlaid integrating current controller and the other one bypassed. Note that, the desired current is at that frequency not achievable neither with closed nor with open control loop. Hence the amplifier is at this frequency only accurate for measuring the impedance and not for charging or discharging the battery with high currents.

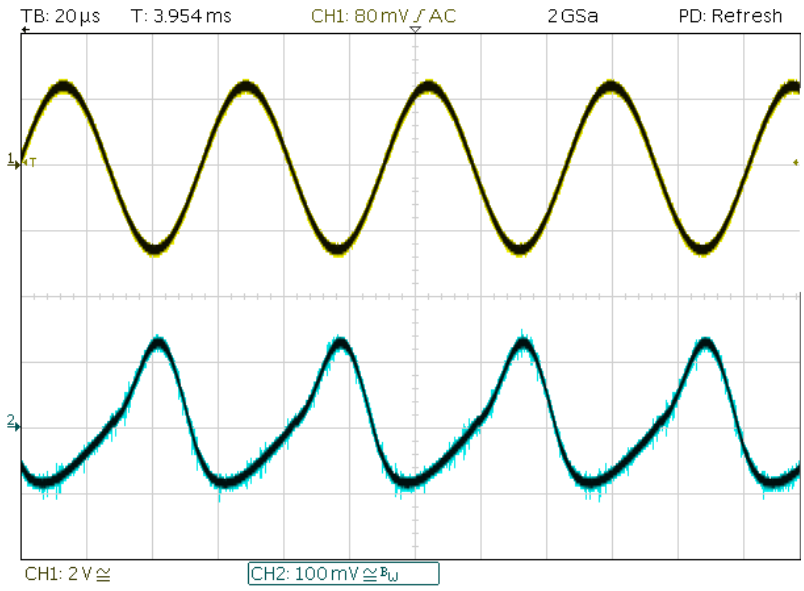

(a) Current controlled

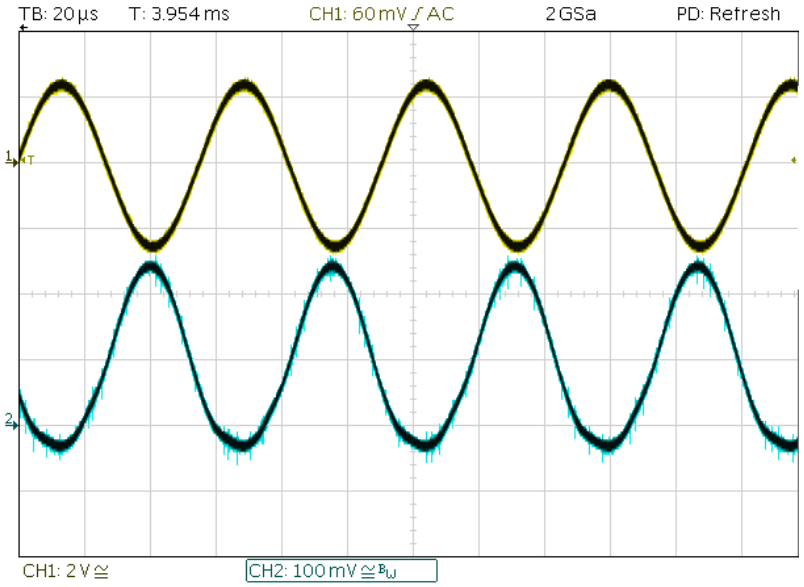

(b) Bypassed integrating controller

Figure 4.4: Sinus reference input signal, Vpp=5 V, f=18 kHz [upper]; measured signal [lower].

The total harmonic distortion was measured to get a more objective comparison about the quality of the amplifier at different frequencies and currents. Further, it provides a base for decision support to use or bypass the overlaid integrating controller. The measurements were done at a battery voltage of 3 V. To measure

the harmonics up to the fourth order we used a spectrum analyzer Agilent 4396B [40, 41, 42, 43]. Because we measured the power directly, we only needed to convert the values from logarithmic to linear domain before using the following equation:

$$k = \sqrt{\frac{P_2 + P_3 + P_4}{P_1 + P_2 + P_3 + P_4}} \tag{4.1}$$

The derived values are listed in table 4.1. Generally, the use of the controller is essential in low frequencies (lower 50 HZ), whereas at high frequencies (higher 15 kHz) the performance deteriorate if the controller is used. The border can be set around 10 kHz depending on the wanted current.

Table 4.1: Total harmonic distortion factor comparison at different frequencies and currents. The left column contains the distortion factors obtained with activated controller and the right column with deactivated controller.

Frequency	$I_{nom_{PP}}$	Distortion factor	
		with controller	without controller
50Hz	2A	0,15%	0,92%
	20A	0,11%	1,8%
	40A	0,11%	1,8%
1kHz	2A	7,7%	4,2%
	20A	5,8%	8,8%
	40A	4,6%	7,4%
10kHz	2A	16%	20%
	20A	8,7%	8,5%
	40A	7,7%	7,5%
20kHz	2A	33%	10%
	20A	37%	12%
	40A	53%	11%

4.2 Low distortion power amplifier in combination with the control unit

Measurement setup

The measurement setup is the same as the proposed one in chapter 3, figure 3.1. The low distortion power amplifier gets its reference signal from the measurement and control unit, whereas the measurement and control unit is connected to the PC

and controlled via the hyper terminal HTerm. The power supply is provided by a HAMEG Triple Power Suplpy HM7042-5[44] (for the ± 15 V) and a HP DC Power Supply 6012B [45] (for the +5 V, 50 A). A high power lithium-ion APR18650M1A[46] from A123Systems acted as device under test. The cell has a nominal capacity of 1.1 Ah and a voltage of 3.3 V. Due to the small size of the cell, only two of the four available temperature sensors are attached to the cell. Figure 4.5 shows the measurement setup in reality.

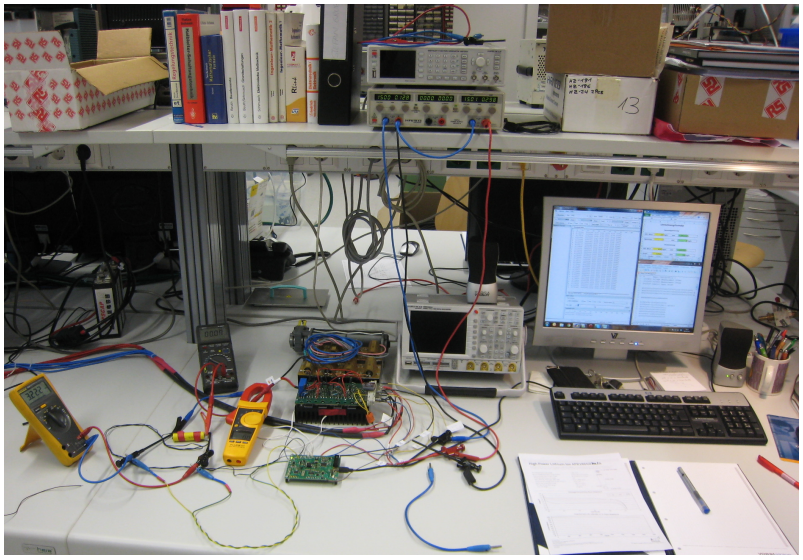

Figure 4.5: Measurement setup of the low distortion power amplifier in combination with the control unit.

Measurements

The measurement noise of the battery voltage is mostly a combination of the crosstalk on the wires (from the battery clamps to the signal conditioning circuit), the component noise of the resistors, capacitors and the differential amplifer used in the signal conditioning circuit and the ADC (PCM4222) quantization noise. The measurement noise of the battery current is a combination of the just mentioned points of the battery voltage, the noise of the current transducer LEM LA55-P and the noise of the used shunt resistor to transform the current signal into a voltage signal.

The quantization noise of an ADC is given by the following equation:

$$\frac{1}{\sqrt{12}} \times \frac{measurement\,range}{2^{number\,of\,bits} - 1} \tag{4.2}$$

Hence, the used 24 bit ADC with a measurement range of ± 5.6 V and ± 50 A has a quantization noise of 193 nV and 1.7 µA.

A first estimation of the measurement noise was done by measuring a constant voltage of 2.275 V (the battery was replaced by three supercaps each 2400 F connected in series). Therefore, the battery current is adjusted to zero using a Keithley 2100 6 1/2 Digit Multimeter [47]. A series of 130.000 samples at a sample rate of 1 kHz was recorded with the control and measurement unit and the standard deviation was determined to 36.5µV and 342.8µA. Hence, the measurement noise is bigger than the quantization noise of the ADC by a factor of 55 for the voltage and 58 for the current. Figure 4.6 depicts the Q-Q plot of the voltage (left) and the current (right) samples compared to their standard deviation.

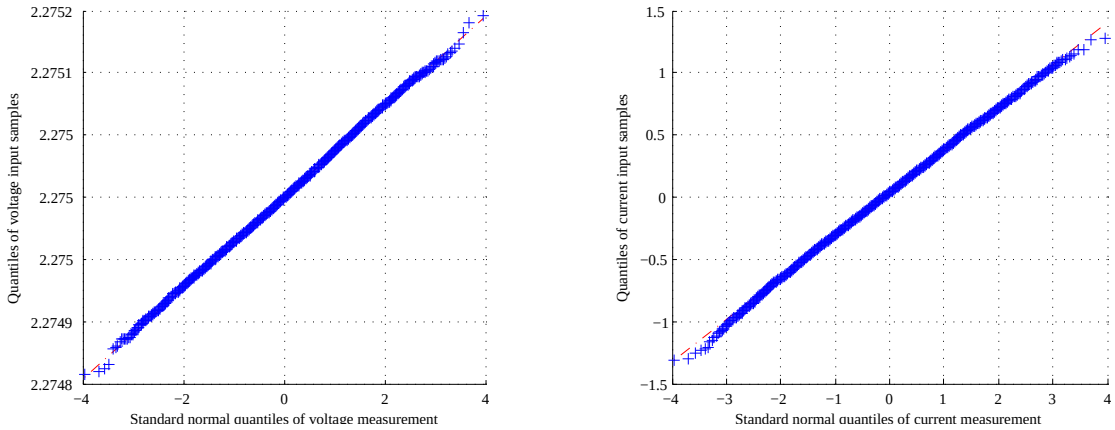

Figure 4.6: Q-Q plot of the voltage (left) and the current (right) samples compared to their standard deviation. 130,000 Samples (130 sec with a sample rate of 1 kHz) of 3 super caps in series at 2.275 V.

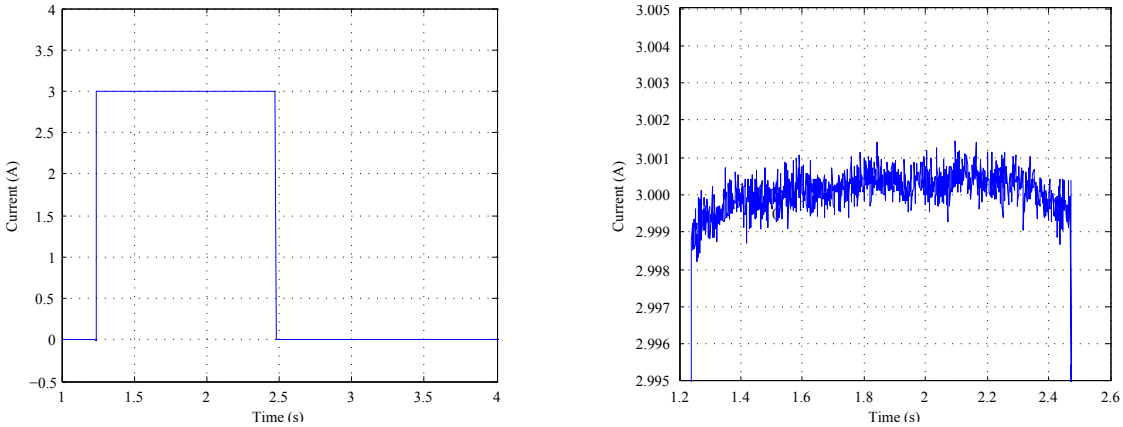

Figure 4.7: Pulse with 3 A for 1.2 s applied to a lithium-ion cell APR18650M1A, 1.1Ah (left). Zoomed view (right).

The next experiment was done to demonstrate the behavior of the system regarding to pulses. Therefore, a pulse with 3 A for 1.2 s was applied to the lithium-ion

cell. The battery voltage and current have been measured at a sample rate of 1 kHz. Figure 4.7 illustrates the measured current signal. The zoomed view shows a current swing of about ±1 mA which fits well to a total measurement range of ±50 A.

The manufacturer of the test lithium-ion cell recommends for charging a CCVC regime with a maximum charge current of 1.5 A and a fast charge current of 4 A. Figure 4.8 depicts the charging with a charge current of 3 A and a charge end voltage of 3.6 V. The charger acts appropriate and keeps the current constant at 3 A as long as the charge end voltage has been reached. At the desired charge end voltage, the controller reduces the current constantly with an unexpected swing of about 0.2 A. Figure 4.9 illustrates the discharging with a discharge current of 6 A and a cut-off voltage of 2 V.

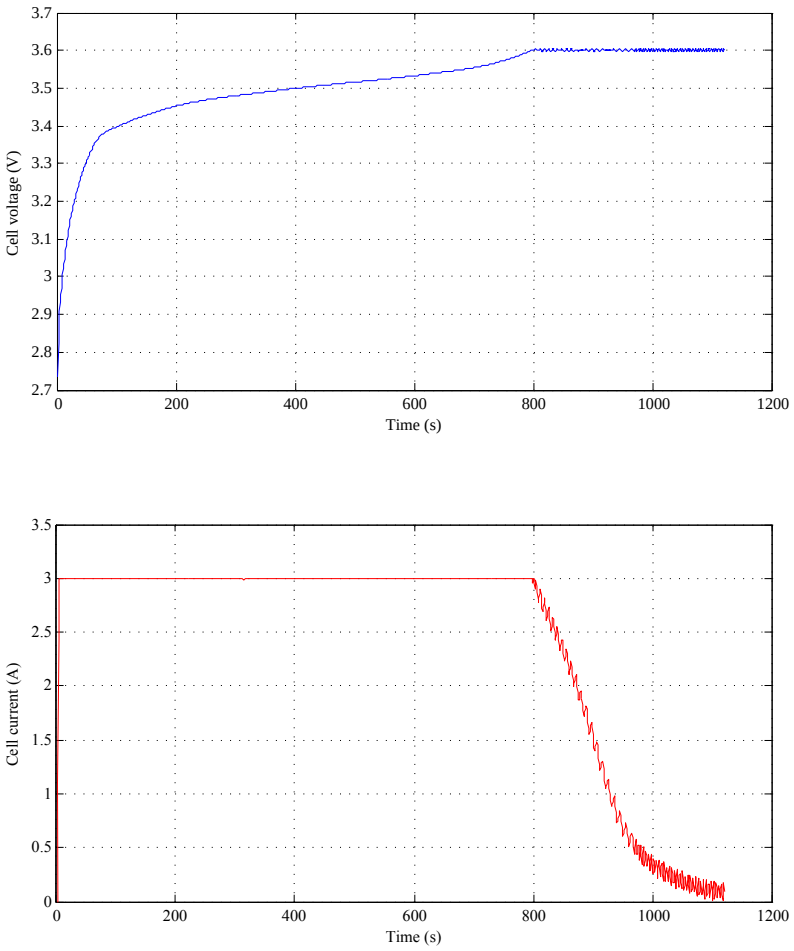

Figure 4.8: Charging a lithium-ion cell APR18650M1A with CCVC regime at maximum charging current of 3 A to a charge end voltage of 3.6 V.

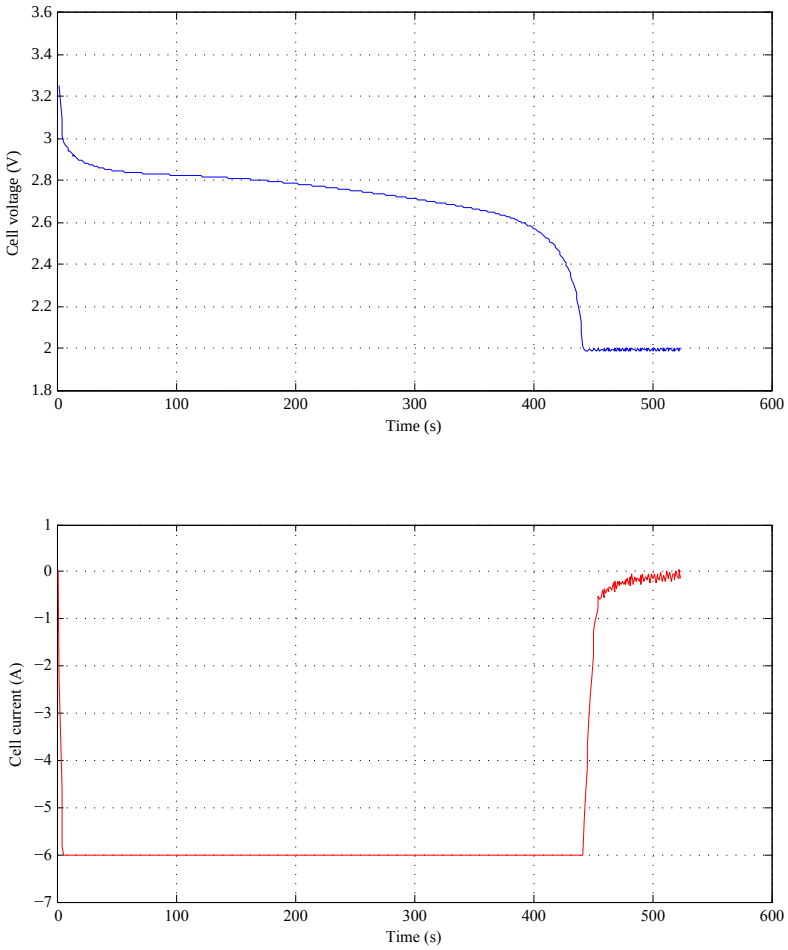

Figure 4.9: Discharging a lithium-ion cell APR18650M1A (SOC = 100 %) to a cut-off voltage of 2 V with a maximum discharge current of 6 A.

4.3 IS measurement with a LiFePo4 battery cell

This subsection shows an example of a measurement procedure in which the required measurement data for the impedance spectroscopy are adopted. This data can further be used for parameter identification to calculate a model of a battery cell as it is shown in 2.2.

Measurement setup

The experiment was done with a battery cell type ANR26650M1A from A123Systems Inc [48]. The cell has a nominal capacity of 2.3 Ah and a nominal voltage of 3.3 V. In

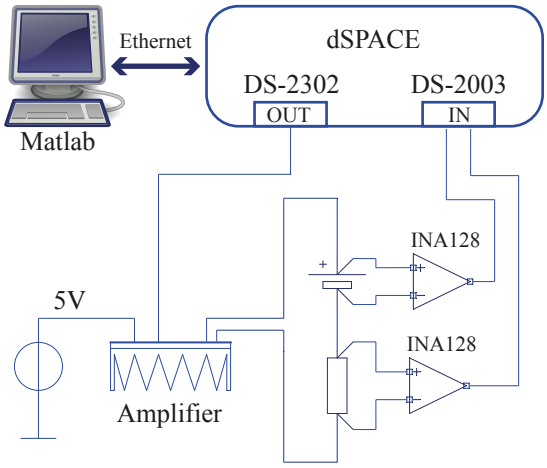

Figure 4.10: Measurement setup of the power amplifier in combination with a dSPACE control and measurement system.

figure 4.10 the principle measurement setup is displayed. The amplifier is powered with 5 V by an usual laboratory power supply unit. The input signal for the amplifier is generated by a dSPACE DS-2302 unit. The cell voltage and current are measured by a dSPACE DS-2003 unit. The dSPACE unit contains a digital signal processor and communicates via Ethernet with a personal computer. A Matlab program serves as automated control for the dSPACE system. The measured data is stored in a text file and is later processed by the software tool Matlab.

Achieved results

Figure 4.11 shows a single pulse out of a series of 20 pulses. In this case a maximum current deviation of 0.5 mA and a maximum Matlab Simulink cycle time of 1s is leading to an accuracy of 5 ppm for a single pulse charge quantity. Parameters for a basic equivalent circuit diagram of the tested cell can be obtained from the transient cell voltage response by optimizing the model to fit the measured data.

In order to plot the impedance over the frequency it is necessary to measure the change of the voltage at different frequencies. Figure 4.12 displays the acquired current and voltage signal at a frequency of 15.9 mHz. This data is one single measurement point of the whole impedance spectroscopy plot which is shown in figure 4.13.

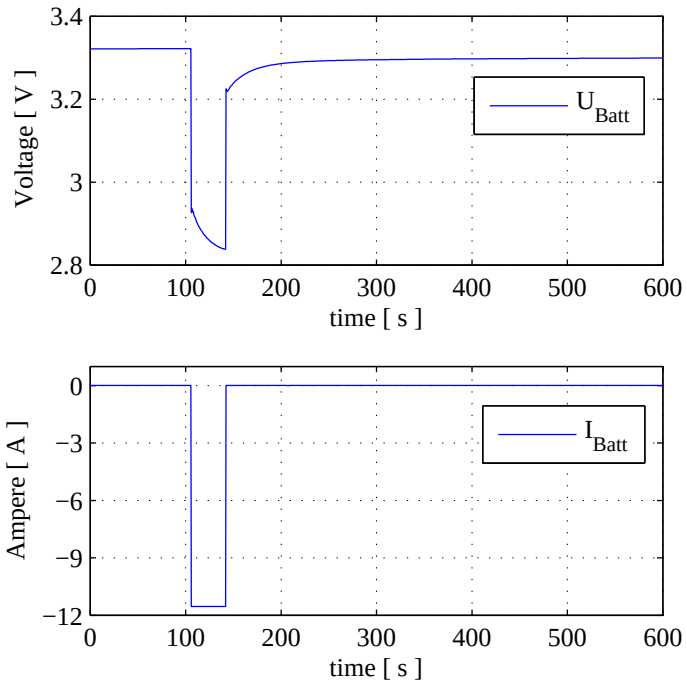

Figure 4.11: Single pulse, I = 11.5 A (≙5 C) at 50 % of State Of Charge.

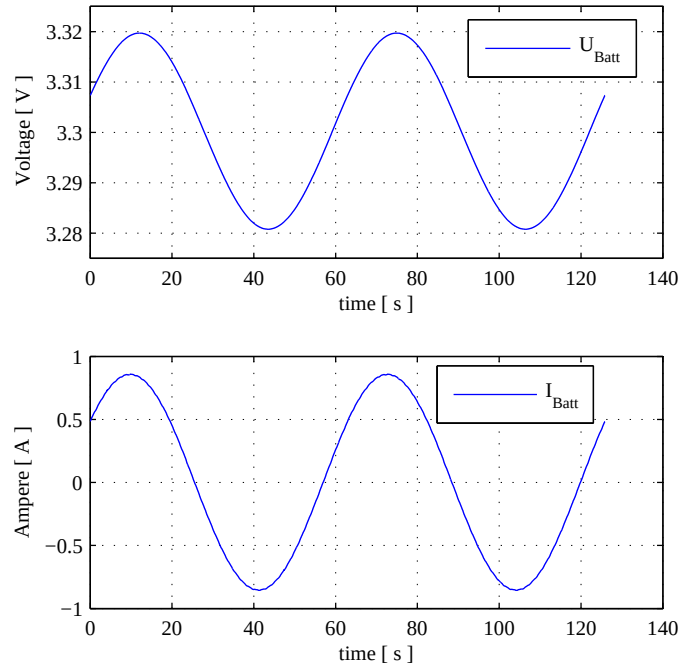

Figure 4.12: Single plot of the cell voltage and current at a frequency of 15.9 mHz.

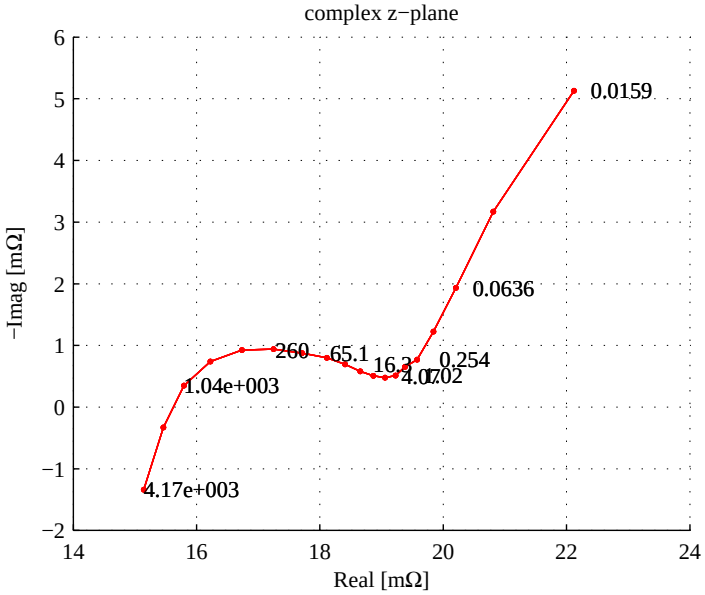

Figure 4.13: Impedance plot over a frequency range from 15 mHz to 4 kHz of a lithium-ion cell, 2300 mAh at a SOC of 50 %. Each data point is a single measurement at the frequency displayed next to it.

4.4 Limitations and suggestions for improvement

Although the realised prototype fulfills most of its objectives as shown in the experiments, a few suggestions for improvement will follow in this section.

The ADC PCM4222 has a sampling rate of 44 kHz. The STM32F103RCT is capable of processing the datapackages. Due to problems with the USB/VirtualComPort transfer rate, the measured data can only be transmitted to the PC with a rate of 1 kHz. In order to increase the transfer rate either a faster USB communication should be established or the size of the Data-Messages should be reduced. For instance, the temperature values will be send every second instead of every millisecond.

The controller which is implemented in the software shows reasonable characteristics in terms of pulses, although the current swing of several mA at the end of a CCVC charging scheme needs to be reviewed.

At the moment the prototype consists of two seperate PCBs. A combination of both in one prototype could significantly decrease the measurement noise.

A graphical user interface, for instance Matlab, would enhance user friendliness in terms of calibrating the system and decreasing errors which will occur in situations when working is based on messaging.

5 Conclusion

This thesis deals with the design, development and realisation of a battery test equipment that is capable of charging and discharging (± 50 A) a single cell, as well as measuring the battery voltage and current in a wide frequency range (50 µHz - 10 kHz) for impedance spectroscopy purpose. The requirements for the prototype are defined in section 1.1. Furthermore, the necessary basics of batteries and a short overview of the impedance spectroscopy in terms of battery modeling are explained in chapter 2. The realised prototype consists of two parts, the low distortion power amplifier and the control and measurement unit which are explained in chapter 3. The amplifier is fed by a reference signal that is amplified in order to charge and discharge the battery. Section 3.2 is concerned with the hardware development and related implementation aspects of the low distortion power amplifier. However, the hardware of the control and measurement unit which generates the amplifier reference signal and measures the temperature, battery voltage and battery current is described in section 3.3. Moreover, the implemented software on the STM32F103RCT microcontroller as well as the communication with the PC are explained in section 3.4. Chapter 4 shows experiments with the prototype to verify the measurement results. Section 4.1 covers the capability and limitations of the low distortion power amplifier, whereas section 4.2 deals with the complete system. Finally, limitations of the current prototype are illustrated and recommendations for an advanced prototype are made in 4.4

Appendix

Low distortion power amplifier

Figure 5.1 to 5.4 show the schematics of the realised prototype of the low distortion power amplifier . The software tool Eagle 5.9 was used to draw the schematics as well for the routing of the PCB.

Control and measurement unit

Figure 5.5 to 5.9 show the schematics of the realised prototype of the control and measurement unit. The software tool Eagle 5.9 was used to draw the schematics as well for the routing of the PCB.

Figure 5.10 illustrates the PCB and provides additionally information of the jumper settings.

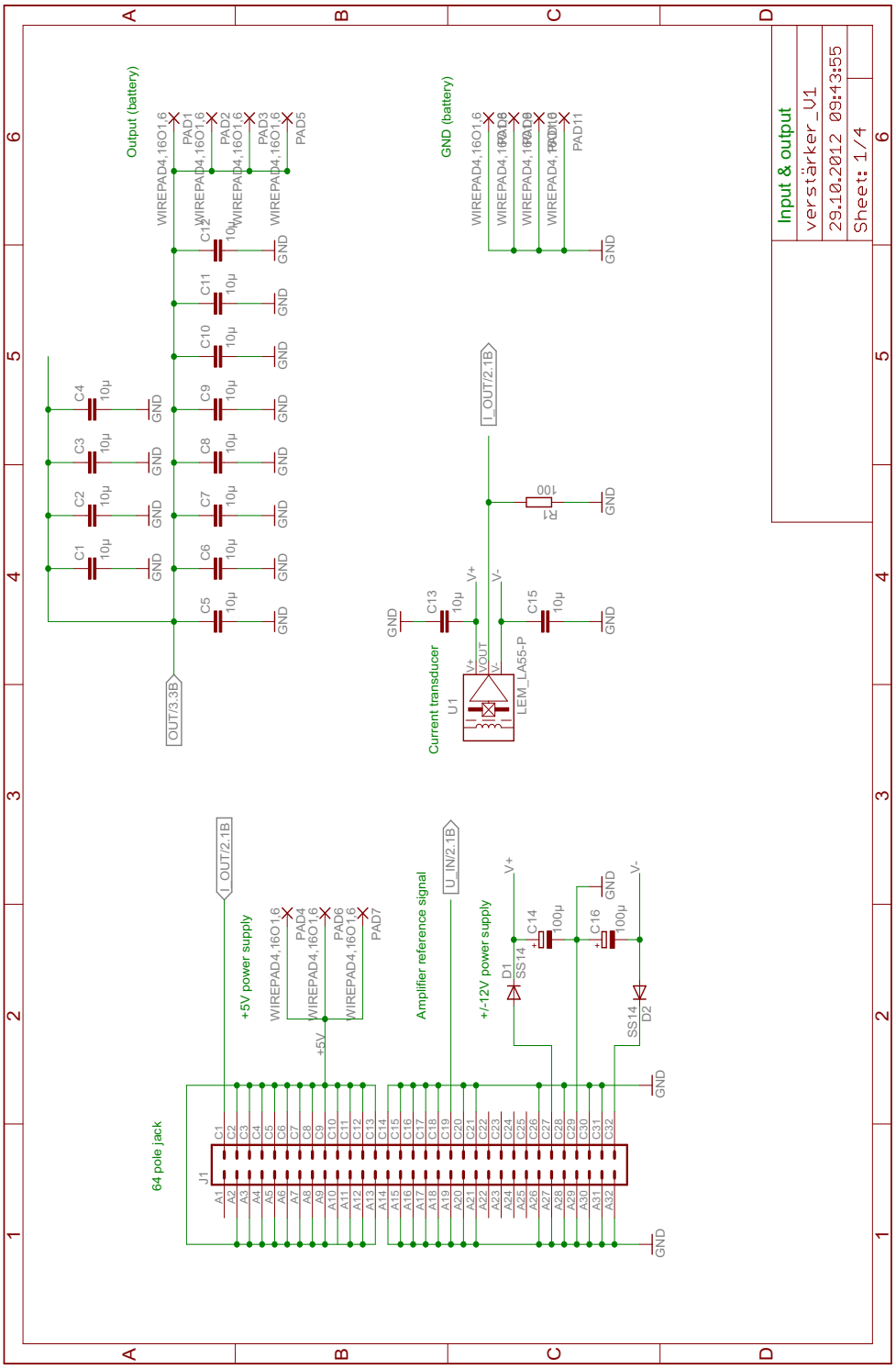

Figure 5.1: Schematic - Low distortion power amplifier: 64-pole jack and current transducer LEM

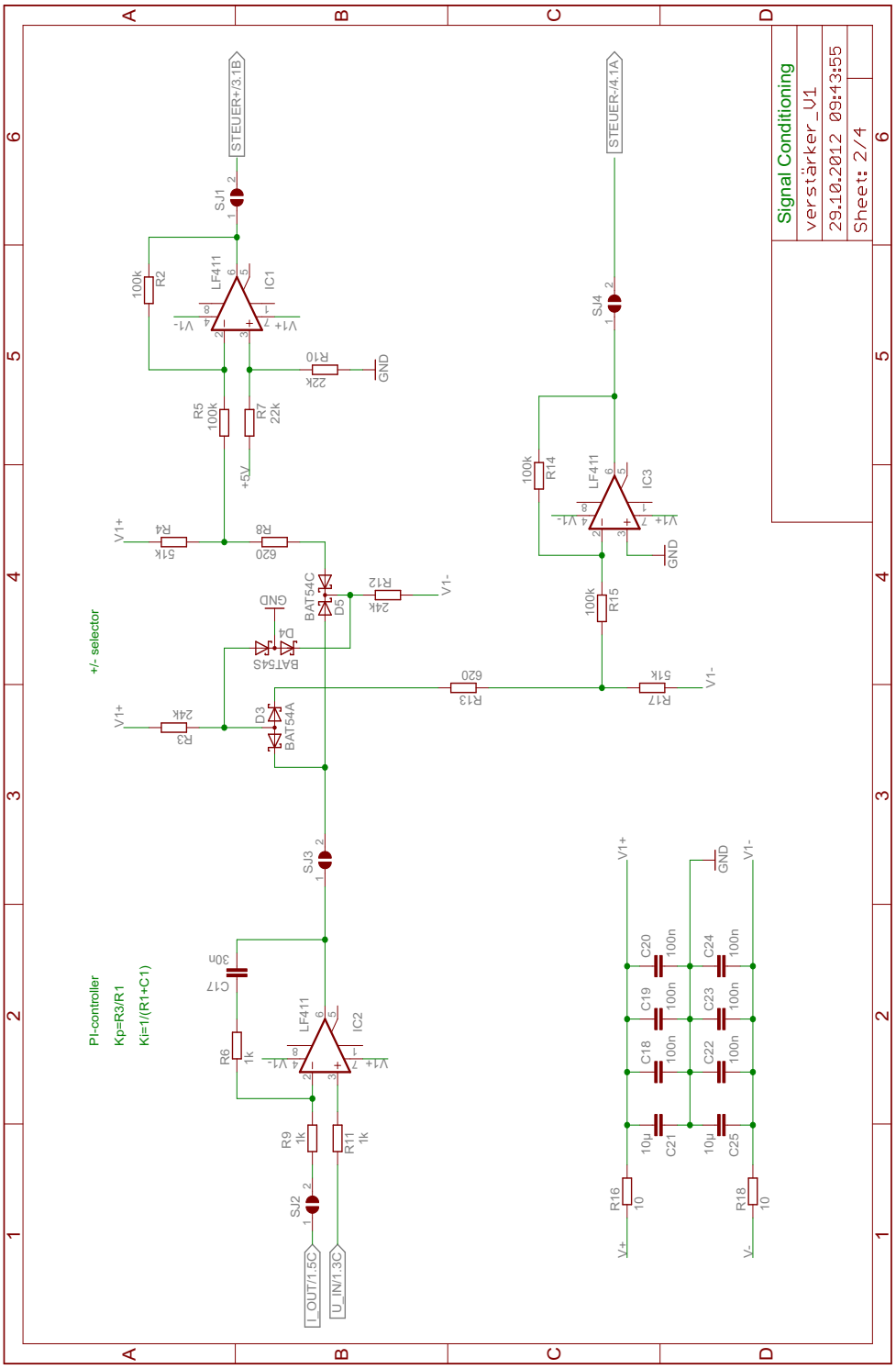

Figure 5.2: Schematic - Low distortion power amplifier: PI-controller, +/- selector, signal processing for the positive and negative stage.

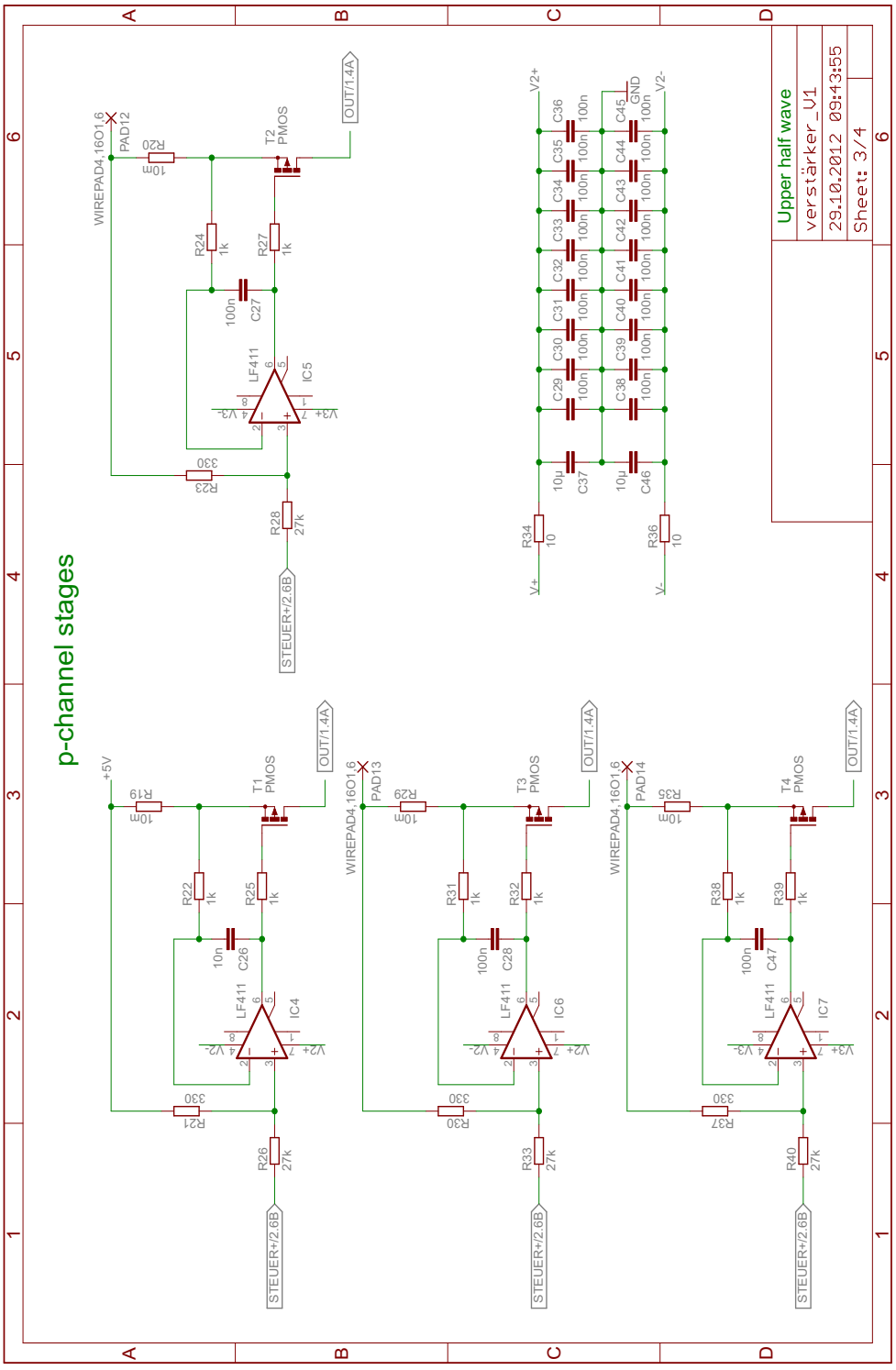

Figure 5.3: Schematic - Low distortion power amplifier: p-channel stages

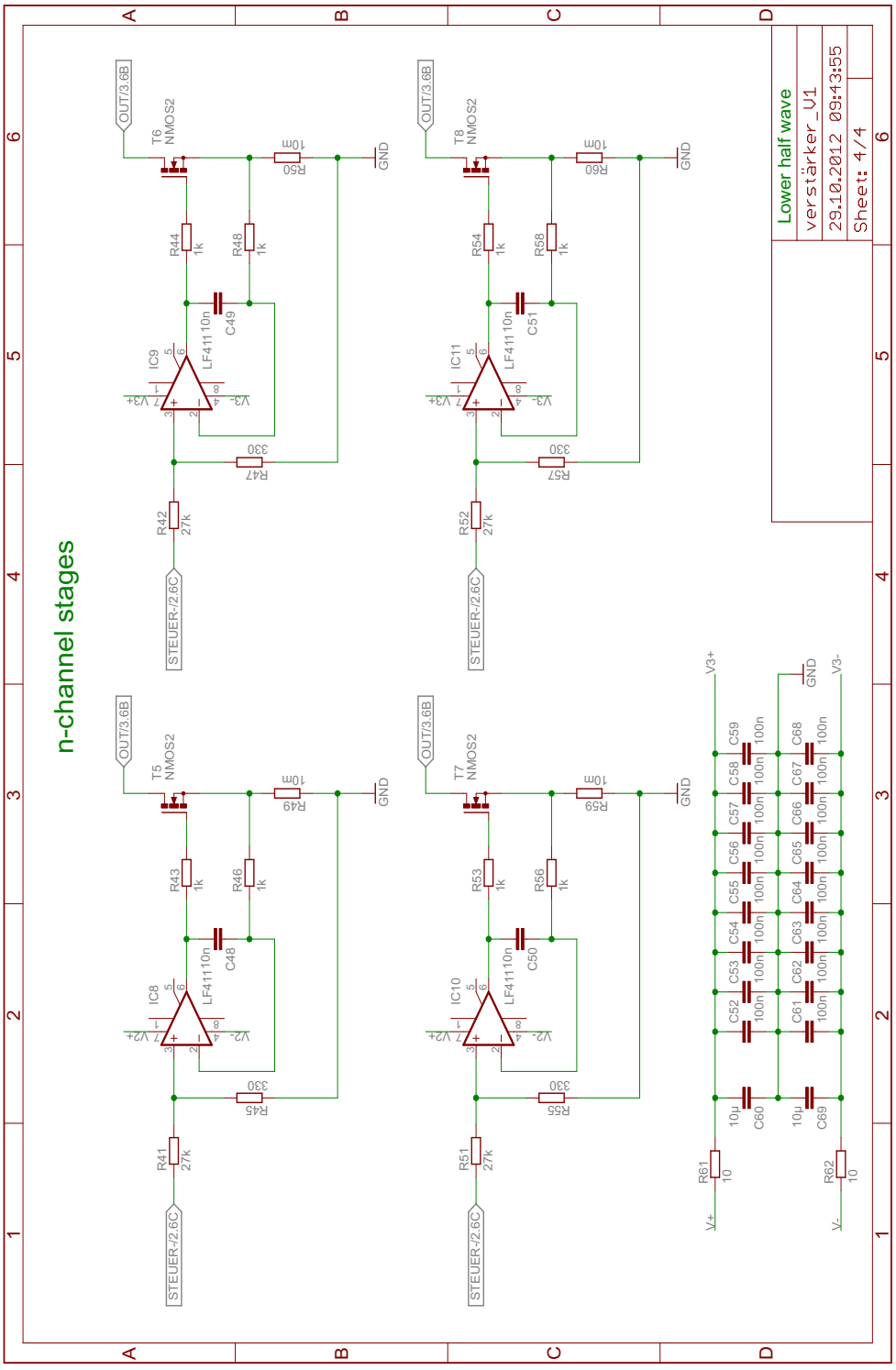

Figure 5.4: Schematic - Low distortion power amplifier: n-channel stages

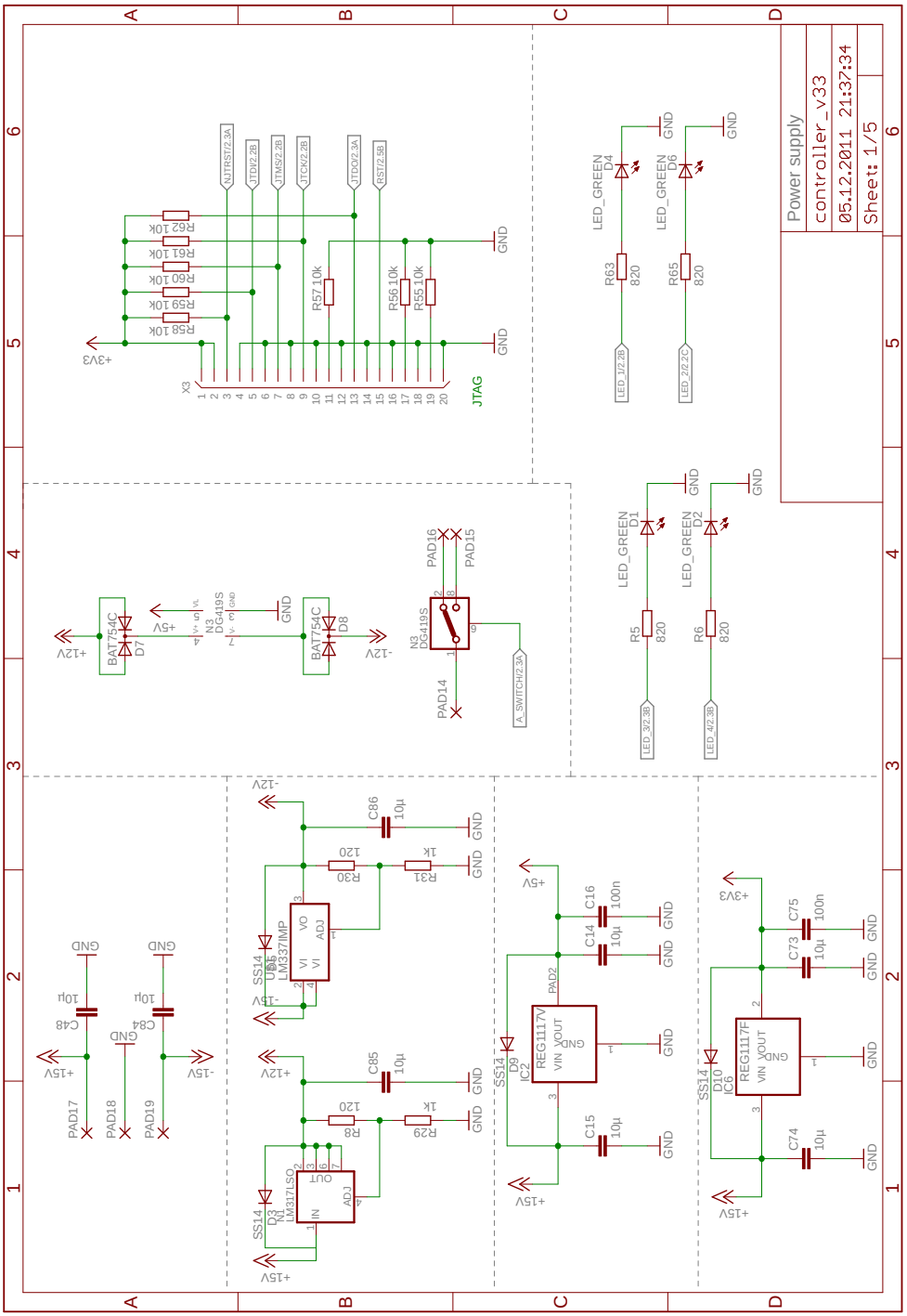

Figure 5.5: Schematic - Control and measurement unit: power supply, analog switch, LEDs, JTAG connector

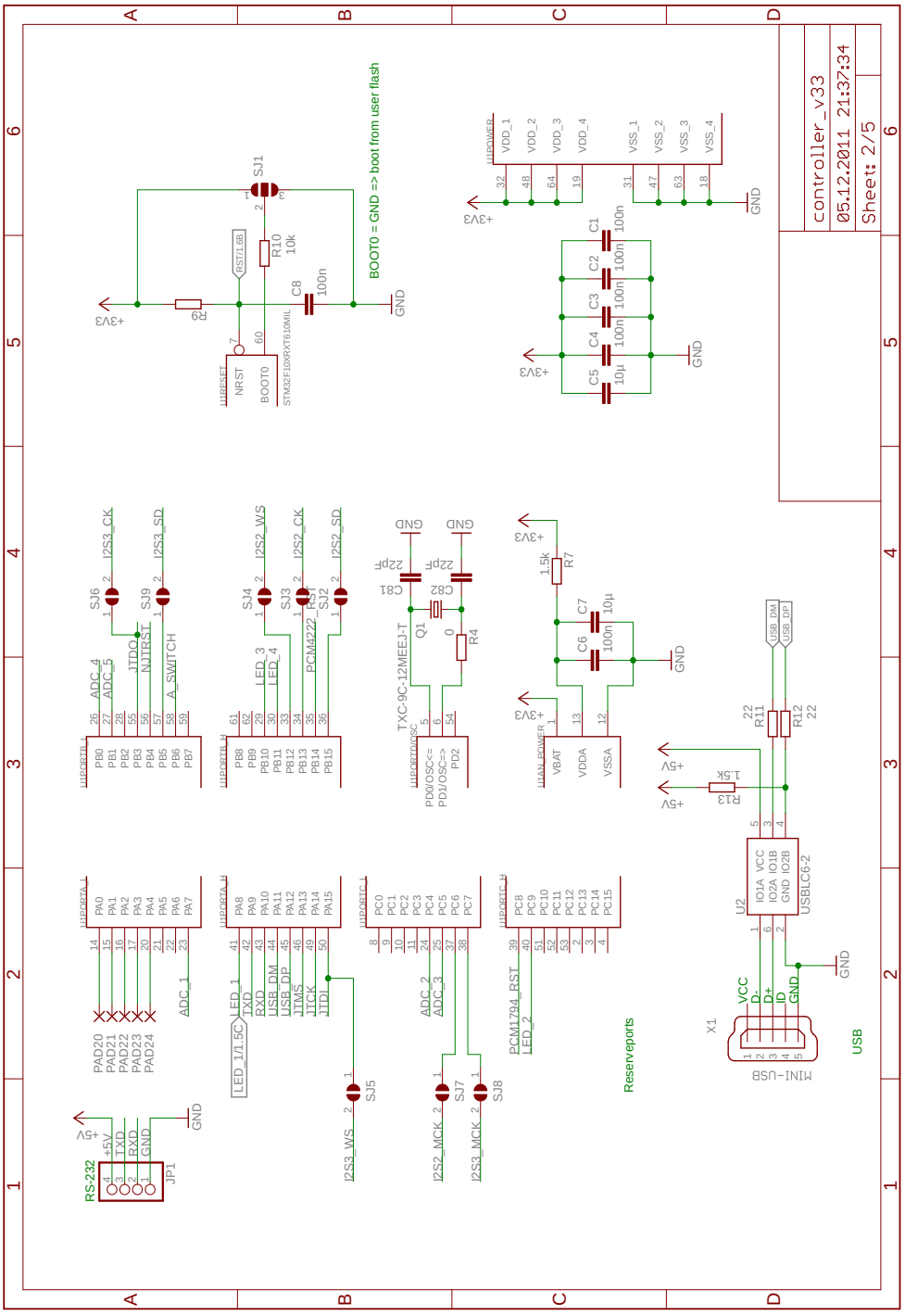

Figure 5.6: Schematic - Control and measurement unit: STM32F103RCT micro controller, USB connector

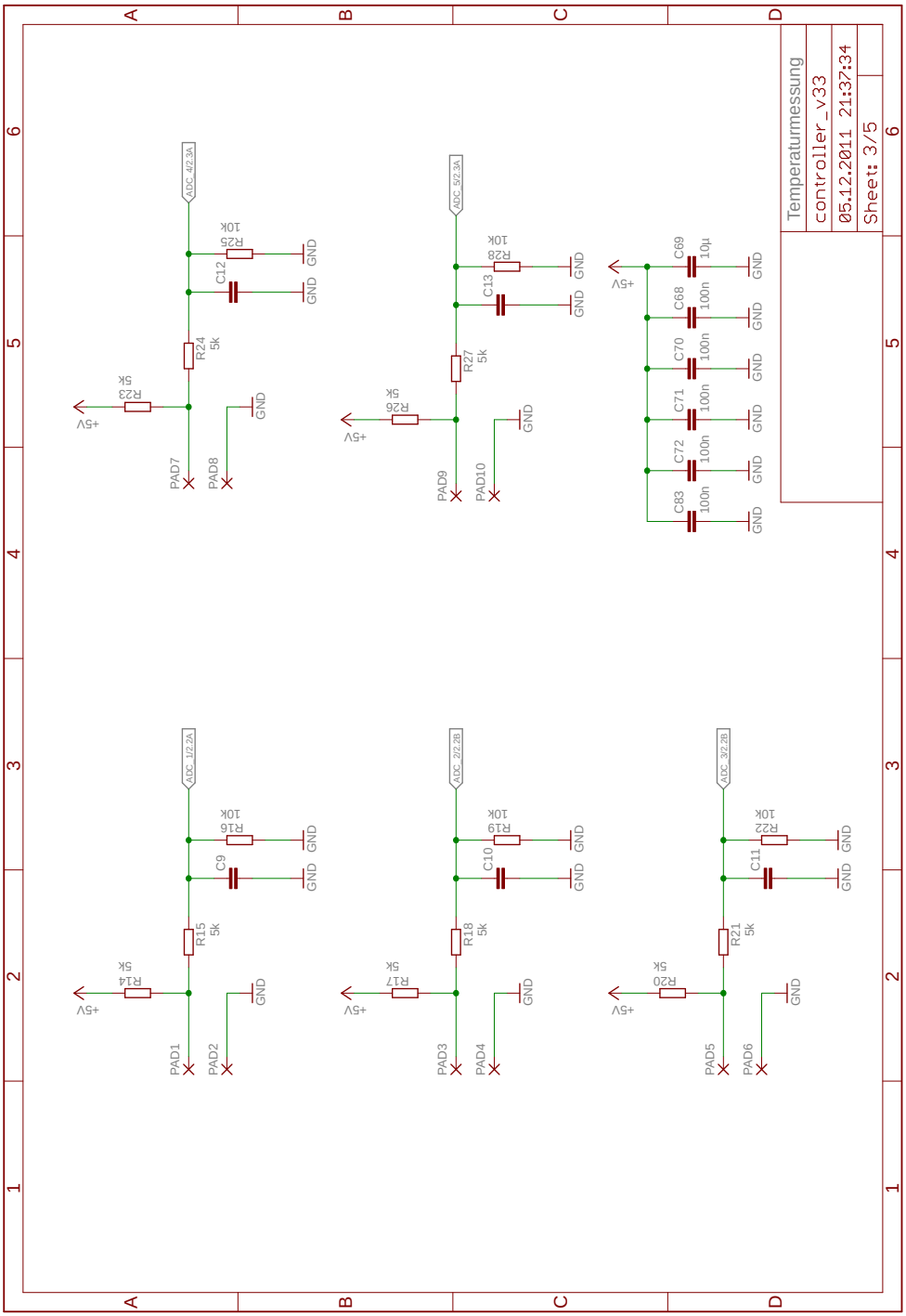

Figure 5.7: Schematic - Control and measurement unit: temperature measurement

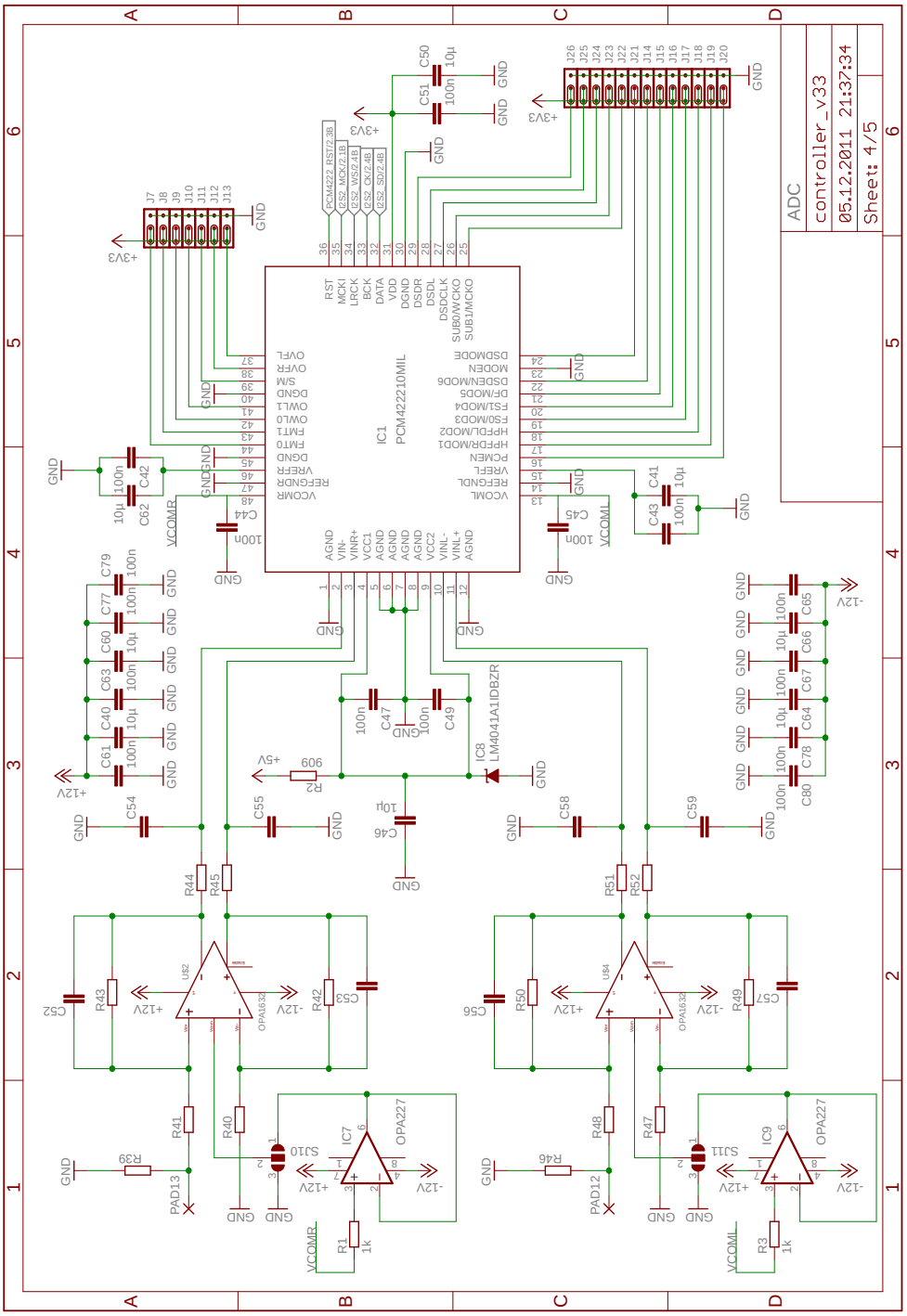

Figure 5.8: Schematic - Control and measurement unit: Battery voltage and current measurement with ADC PCM4222

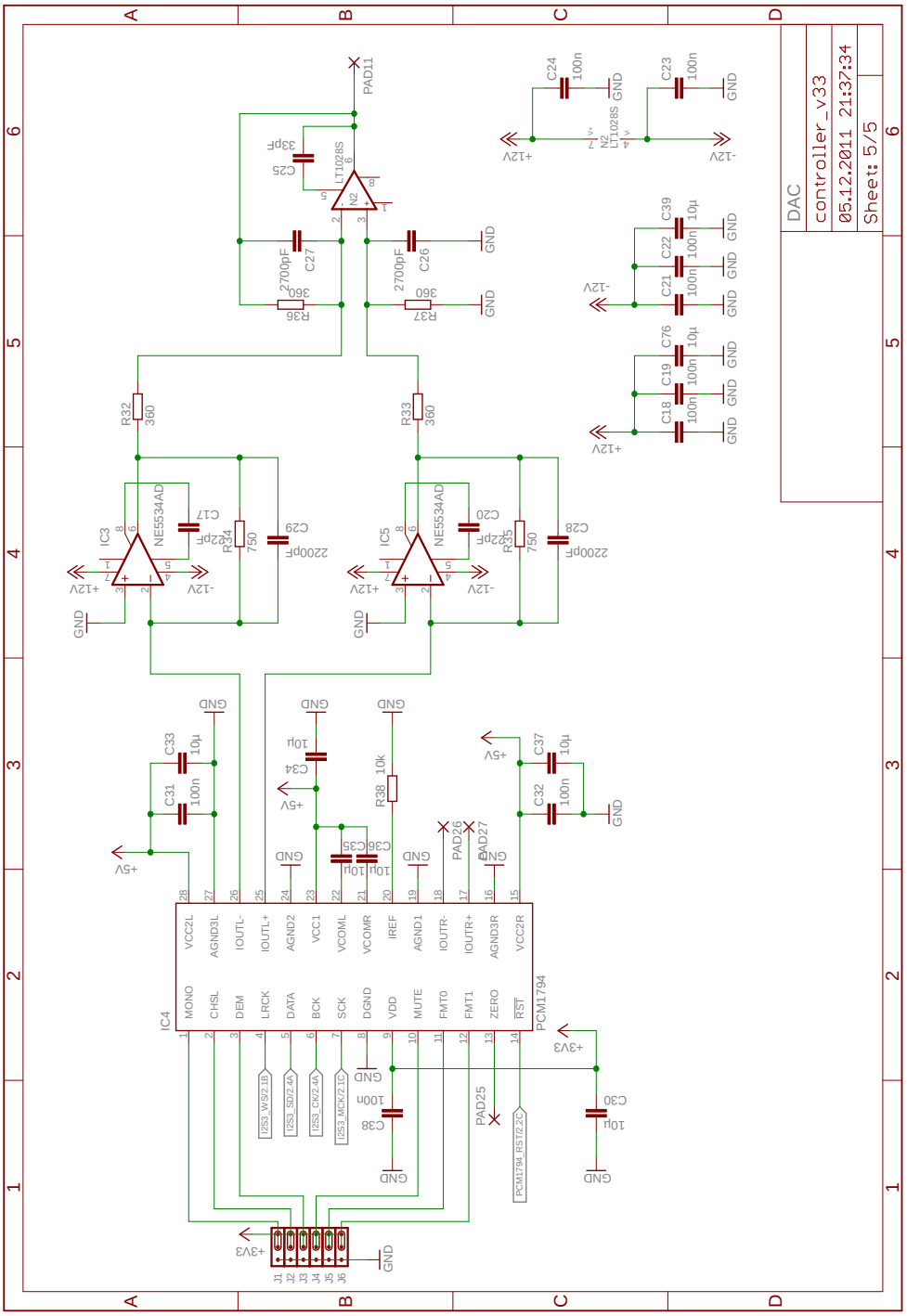

Figure 5.9: Schematic - Control and measurement unit: Amplifier voltage reference signal generation with DAC PCM1794

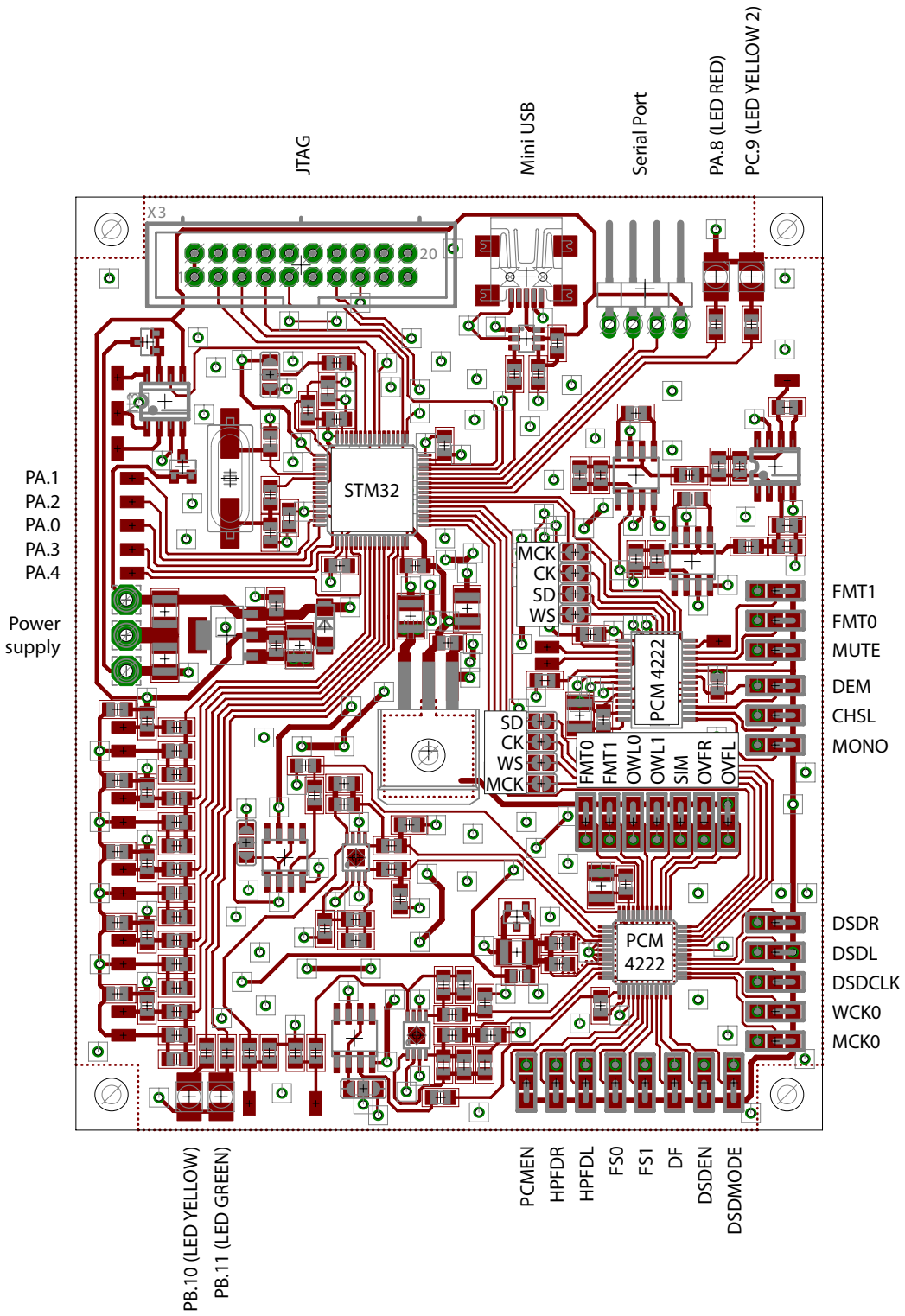

Figure 5.10: PCB and jumper description of the control and measurement unit.

Software description

Figure 5.11 and 5.12 list all possible messages that can be sent or received by the control and measurement unit.

The columns (from left to right) are:

- [x]
  Depicts the start character/position of the command or information within in the received/transmitted message.
- NOC
  Number of characters of the command or information.
- Description
  Short description of the command or information.
- Possible States
  The possible states can be just a character or a number within a certain range.
- Variable Name
  This is the storage/variable name of the command or information in the programmed software.
- Size
  Shows the used data type of the variable in the programmed software.

USB - Messages

[x]	NOC	Description	Possible States	Variable Name	Size
Stop - Message					
0	1	Stop-Message Prefix	H		
1	1	What	A (All), S (Signal), M (Meassurement)		
2	1	How	D (Delete all configurations), N (No, don't delete the configurations)		
3	1	When	I (Immediate), C (Configuration)		
Configuration					
3	3	Number of configuration, at that end the system will be stopped	0-200		
Configuration - Message					
0	1	Configuration-Message Prefix	C		
1	1	Analog Switch - closed or open loop	C (Closed), O (Open)	AnalogSwitch	uint8_t
2	1	Operating mode	P (Pulse), S (Sinus), C (Charge) D, (Discharge)	SignalType	uint8_t
Pulse					
3	8	Current	-8388608 to +8688607 (24Bit ADC Value) (-50.000mA bis +50.000mA)	PulseCurrent	int32_t
11	10	On-Time	0-4294967296ms (uint32_t)	PulseTimeOn	uint32_t
21	10	Off-Time	0-4294967296ms (uint32_t)	PulseTimeOff	uint32_t
31	5	Repetitions	0-65536 (Uin16_t)	PulseRepetitions	uint16_t
Charge					
3	8	Nominal current (maximum loading current)	24Bit ADC Value (0 to +50.000mA)	Charge_Current	int32_t
11	8	Charging voltage (voltage up to that will be loaded)	24Bit ADC Value (0 to +5.600mV)	Charge_Voltage	int32_t
19	8	End current (current from that on the end time is running)	24Bit ADC Value (0 to +50.000mA)	Charge_EndCurrent	int32_t
27	7	End time	0-4294967296ms (uint32_t)	Charge_EndTime	uint32_t
Discharge					
3	8	Nominal current (maximum discharge current)	24Bit ADC Value (0 to -50.000mA)	Discharge_Current	int32_t
11	8	Discharge voltage (voltage down to that will be discharged)	24Bit ADC Value (0 to +5.600mV)	Discharge_Voltage	int32_t
19	8	End current (current from that on the end time is running)	24Bit ADC Value (0 to +50.000mA)	Discharge_EndCurrent	int32_t
27	7	End time	0-4294967296ms (uint32_t)	Discharge_EndTime	uint32_t
Sine					
3	7	Amplitude current	23Bit ADC Value (0 to +50.000mA)	Sine_Amplitude	uint32_t
		Frequency	0-4294967296µHz (uint32_t)	Sine_Frequency	uint32_t
		Repetitions	0-65536 (Uin16_t)	Sine_Repetitions	uint16_t
Start- Message					
0	1	Start-Message Prefix	S		
1	4	Number of configuration that will be started	0-200	ActiveConfig	uint8_t

Figure 5.11: Description of possible messages sent and received via USB (part 1)

USB - Messages

[x]	NOC	Description	Possible States	Variable Name	Size
Basic-Configuration - Message					
0	1	Basic-Configuration-Message Prefix	B		
1	5	No. Of steps with 1kHz sample rate	0-65536 (Uin16_t)	BConfig_1kHzSRSteps	uint16_t
6	5	No. Of steps with 100Hz sample rate	0-65536 (Uin16_t)	BConfig_100HzSRSteps	uint16_t
11	5	No. Of steps with 10Hz sample rate	0-65536 (Uin16_t)	BConfig_10HzSRSteps	uint16_t
16	4	Maximum temperature limit of heat sink	0-4096 (12Bit ADC Value)	BConfig_MaxTempHeatSink	uint16_t
20	4	Maximum temperature limit of battery	0-4096 (12Bit ADC Value)	BConfig_MaxTempBattery	uint16_t
24	7	Maximum battery voltage limit	-8388608 to +8688607 (24Bit ADC Value)(0 bis +5.600mV)	BConfig_MaxBatteryVoltage	int32_t
31	7	Minimum battery voltage limit	-8388608 to +8688607 (24Bit ADC Value)(0 bis +5.600mV)	BConfig_MinBatteryVoltage	int32_t
38	5	Slewrate PID controller	0-65536 (Uin16_t)	BConfig_PID_Slewrate	uint16_t
43	5	Integral gain PID controller	0-65536 (Uin16_t)	BConfig_PID_IntegralGain	uint16_t
48	8	Voltage Meassurement Offset	-8388608 to +8688607 (24Bit ADC Value)	BConfig_VoltageOffset	int32_t
56	8	Current Meassurement Offset	-8388608 to +8688607 (24Bit ADC Value)	BConfig_CurrentOffset	int32_t
64	8	Control Input Offset	-8388608 to +8688607 (24Bit ADC Value)	BConfig_ControlInputOffset	int32_t
Error - Message					
0	1	Error-Message Prefix	E		
1	64	Error Message in words	max. 64 characters		uint8_t[64]
Data - Message					
0	1	Data-Message Prefix	D		
1	8	Battery voltage - PCM4222 Left Channel	24Bit in int32_t (-5.600mV bis +5.600mV)	I2S2_ADC_Value_L	int32_t
9	8	Battery current - PCM4222 Right Channel	24Bit in int32_t (-50.000mA bis +50.000mA)	I2S2_ADC_Value_R	int32_t
17	4	Temperature of heat sink	0-4096	TempSensorMean[ITempFlag][0]	uint16_t
21	4	Temperature 1	0-4096	TempSensorMean[ITempFlag][1]	uint16_t
25	4	Temperature 2	0-4096	TempSensorMean[ITempFlag][2]	uint16_t
29	4	Temperature 3	0-4096	TempSensorMean[ITempFlag][3]	uint16_t
33	4	Temperature 4	0-4096	TempSensorMean[ITempFlag][4]	uint16_t
Information-Message					
0	1	Information-Message Prefix	I		
1	64	Information Message in words	max. 64 characters		uint8_t[64]

Figure 5.12: Description of possible messages sent and received via USB (part 2)

Bibliography

[1] Frost & Sullivan. *Global Battery Markets*, 2009. 1

[2] AB 32, Global Warming Solution Act, September 2006. 1

[3] Paul Hughes. *Advanced clean cars summary*, November 2011. 2

[4] PPP European Green Cars Initiativ. *European Roadmap Electrification of Road Transport*, version 2.0 edition, November 2010. 2

[5] David Linden and Thomas B. Reddy. *Handbook of Batteries*. McGraw-Hill, 3rd edition, 2002. 2, 5, 6, 7, 11, 12, 14

[6] Gamry Instruments. *Reference 3000*, October 2012. Specification Sheet. 3

[7] PEC. *SBT0550 Battery Test System*, October 2012. Specification Sheet. 3

[8] Arbin Instruments. *BT2000*, July 2003. Specification Sheet. 3

[9] Maccor. *FRA-0355*, August 2010. Specification Sheet. 3

[10] Maccor. *Series 8500*, July 2012. Specification Sheet. 3

[11] Evgenij Barsoukov and J. Ross Macdonald. *Impedance Spectroscopy : Theory, Experiment, and Applications*. John Wiley & Sons, Inc., 2nd edition, 2005. 5, 15

[12] Texas Instruments. *Battery Charging*, 2011. Application Note. 7

[13] Woodbank Communications Ltd. *Battery Chargers and Charging Methods*, 2005. 7

[14] Battery Association of Japan. *Car Battery Structure*, 2010. 10

[15] Li-Ion Battery, October 2012. 13

[16] Gamry Instruments. *Basics of Electrochemical Impedance Spectroscopy*, 2010. Application Note. 15, 16

[17] Gamry Instruments. *Equivalent Circuit Modeling in EIS*, August 2010. Application Note. 15, 16

[18] Bernhard Schweighofer, Hannes Wegleiter, Martin Sommer, and Manes Recheis. Fast and accurate battery model applicable for system level simulation. In *European Electric Vehicle Congress (EEVC)*, 2011. 16

[19] Bernhard Schweighofer, Hannes Wegleiter, Manes Recheis, and Paul Fulmek. Fast and accurate battery model applicable for ev and hev simulation. In *Instrumentation and Measurement Technology Conference (I2MTC), 2012 IEEE International*, pages 565 – 570, 2012. 16

[20] Walter Meusburger. *A novel power amplifier topology without crossover distortion.* PhD thesis, Graz, University of Technology, 1999. 18

[21] NXP Semiconductors. *BAT754 Schottky barrier diodes*, October 2012. Data Sheet. 19

[22] BI Technologies. *20W TO220 High Power Resistors*, April 2011. Data Sheet. 21

[23] Ulrich Tietze and Christoph Schenk. *Halbleiter-Schaltungstechnik.* Springer, 12th edition, 2002. 21, 22

[24] LEM. *LA 55-P - Current Transducer*, 2012. Data Sheet. 26

[25] Bourns. *PWR2615 100Ohm Shunt*, August 2009. Data Sheet. 26

[26] Texas Instruments. *PCM4222 - High-Performance, 2-Channel, 24-Bit, 216kHz Sampling Multi-Bit Delta-Sigma A/D (Rev. A)*, 2010. Data Sheet. 26

[27] Texas Instruments. *Fully-Differential Amplifiers*, January 2002. Application Note. 26

[28] Texas Instruments. *OPA227 High Precision, Low Noise Operational Amplifiers*, January 2005. Data Sheet. 26

[29] Texas Instruments. *PCM1794 - 24-Bit, 192- kHz Sampling, Advanced Segment, Audio Stereo DAC (Rev. C)*, 2009. Data Sheet. 27

[30] Texas Instruments. *LM135/LM235/LM335, LM135A/LM235A/LM335A Precision Temperature Sensors*, December 2008. Data Sheet. 28

[31] National Semiconductor. *National Semiconductor's Temperature Sensor Handbook*, March 2003. Handbook. 28

[32] STMicroelectronics. *RM0008 STM32F103xx*, January 2011. Reference Manual. 30, 31, 32, 33

[33] Craig.Peacock@beyondlogic.org. *USB in a Nutshell*, May 2002. Manual. 31

[34] USB Implementers Forum, Inc. *Universal Serial Bus Revision 2.0 Specification* , October 2012. Specification. 31

[35] Philips Semiconductors. *I2S bus specification*, June 1999. Specification. 33

[36] Stefan Gruber, Manes Recheis, Bernhard Schweighofer, and Hannes Wegleiter. Low distortion power amplifier for battery measurement systems. In *Instrumentation and Measurement Technology Conference (I2MTC), 2012 IEEE International*, pages 154 – 158, 2012. 36

[37] Hameg Instruments. *HMP4040 - Programmable 3/4 Channel High-Performance Power Supply*, September 2012. User Manual. 36

[38] Hameg Instruments. *HMF2550 - Arbitrary function generator*, October 2012. User Manual. 36

[39] Hameg Instruments. *HMO3524 - Digital Oscilloscope*, September 2012. User Manual. 36

[40] Agilent Technologies. *Agilent 4396B Network/Spectrum/Impedance Analyzer 4396B Network/Spectrum/Impedance Analyzer*, May 2003. User Manual. 40

[41] Agilent Technologies. *Agilent 4396B Network/Spectrum/Impedance Analyzer 4396B Network/Spectrum/Impedance Analyzer*, February 2008. Reference Guide. 40

[42] Agilent Technologies. *Agilent Spectrum Analysis Basics*, August 2006. Application Note. 40

[43] Agilent Technologies. *8 Hints for Better Spectrum Analysis*, September 2009. Application Note. 40

[44] Hameg Instruments. *Triple Power Supply HM7042-5*, September 2009. Data Sheet. 41

[45] Agilent Technologies. *HP 6012B DC Power Supply 0-60V / 0-50A, 1000W*, April 2004. Data Sheet. 41

[46] A123 Systems. *High Power Lithium Ion APR18650M1A*, April 2009. Data Sheet. 41

[47] Kethley Instruments. *Keithley 2100 6 1/2 Digit Multimeter*, December 2011. Data Sheet. 42

[48] A123 Systems. *A123 ANR26650M1A rechargable litihium ion cell*, April 2009. Data Sheet. 44

Nomenclature

µC	Microcontroller
ADC	Analog to Digital Converter
CCVC	Current Controlled Voltage Controlled Is a charging regime particularly for lithium-ion batteries.
CPU	Central Processing Unit
DAC	Digital to Analog Converter
DC	Direct Current
EV	Electric Vehicle
HEV	Hybrid Electric Vehicle
I^2S	Inter-IC Sound or Integrated Interchip Sound It is an electrical serial bus interface standard used for connecting digital audio devices together.
IRQ	Interrupt Request
IS	Impedance Spectroscopy
LED	Light Emitting Diode
NVIC	Nested Vectored Interrupt Controller
OPA	Operational Amplifier
PC	Personal Computer
PCB	Printed Circuit Board
PDA	Personal Digital Assistant
PHEV	Plug-in Hybrid Electric Vehicle
SLI	Starting Lighting Ignition

SOC	State Of Charge
UPS	Uninteruptible Power Systems
USB	Universal Serial Bus